Thin film microfluidic reactors in electrochemical advanced oxidation processes for wastewater treatment: A review on influencing parameters, scaling issues and engineering considerations

Faidzul Hakim Adnan, Marie-Noëlle Pons, Emmanuel Mousset

Thin film microfluidic reactors in electrochemical advanced oxidation processes for wastewater treatment: A review on influencing parameters, scaling issues and engineering considerations

Faidzul Hakim Adnan[1], Marie-Noëlle Pons[1,2], Emmanuel Mousset[1,*]

[1] *Université de Lorraine, CNRS, LRGP, F-54000 Nancy, France*

[2] *LTSER-LRGP, CNRS, Université de Lorraine, F-54000 Nancy, France*

ACCEPTED IN

***ELECTROCHEMICAL SCIENCE ADVANCES* JOURNAL**

(in Special issue from ESEE 2021 congress)

*Contact of corresponding author: emmanuel.mousset@cnrs.fr

Abstract

The use of microfluidic electrochemical reactors has been introduced several decades ago, but their application in the field of wastewater treatment is more recent (2010). The parallel development of electrochemical advanced oxidation processes (EAOPs) as promising technologies for effluent treatment make them good candidates to be implemented as thin film cells. This allows favoring the mass transfer, which is particularly interesting for heterogenous electro-oxidation. Moreover, the energy requirement is reduced, while there is possibility to treat low-conductivity solutions. This review intends to provide instructions on the main operating parameters to be optimized during the EAOPs treatment. Directions on engineering aspects have been given to overcome the main drawbacks of microreactors such as fouling, scaling and low treatment capacity, based on recent encouraging results given in literature. The promising development of hybrid processes that combine electro-separation with electro-conversion would also benefit from such reactor designs.

Keywords

Anodic oxidation; Electro-Fenton; Electro-precipitation; Interelectrode distance; Reactive electro-mixing

1. Introduction

Within the framework of water reuse as a countermeasure against water scarcity that might concern a large number of countries across the globe, conventional biological and physicochemical treatments applied in wastewater treatment plants (WWTPs) do not suffice [1, 2]. In response, a variety of complementary treatments has been proposed across literature and some of them even have been applied at industrial scale [3-6]. The majority of them are based on the fundamentals of chemical oxidation, in which strong oxidants are involved in the degradation of pollutants [7, 8]. Classical processes such as chlorination, ozonation and advanced oxidation processes (AOPs) are to an extent well-established to be able to totally degrade organic contaminants present in aqueous media [3, 9]. Nevertheless, their efficiency comes first and foremost with high operational price [10]. Secondly, the addition of chemicals into the media to be treated is a prerequisite, be it H_2O_2, Cl_2, O_3, acid/base and/or ferrous sources. One might notice the contradictory practices between preserving the aquatic ecosystem receiving the treated wastewater against the admittance of unnatural substances into it when chemical reagents are introduced into the media to be treated [11].

AOP techniques have been doped by the introduction of electrochemical advanced oxidation processes (EAOPs) [12-14]. The latter have been documented across literature to also be able to degrade organic pollutants into simpler organic compounds which are easier to be biodegraded [15-18]. A quasi-complete mineralization into CO_2 and inorganic species can even be obtained if required [19, 20]. A huge boost to the limitation of AOPs is that EAOPs do not necessarily require the addition of chemicals to electrogenerate strong, quasi non-selective oxidizing agent such as hydroxyl radicals ($^{\bullet}OH$) as well as hydrogen peroxide (H_2O_2) *in-situ* [21].

In addition to the advanced electro-oxidation by $^{\bullet}OH$ mentioned above, other indirect electro-oxidation (also called mediated electro-oxidation) can take place with active oxidants ($HClO/ClO^-$, Cl_2, O_3, etc.) depending on the composition of electrolyte [22-25]. It exists other variants of EAOPs such as those where photo-, solar photo- and sono- irradiation sources have been called upon in a way

to optimize the processes [14, 26-28]. The coupling between EAOPs have also been explored to combine heterogeneous and homogeneous $^{\bullet}$OH production to improve treatment capacity [9, 29, 30].

In recent years, the application of submillimetric reactors within the framework of EAOPs has spurred the capability of treatment of wastewater effluent using these techniques [29, 31, 32]. The micrometric interelectrode distance (d_{elec}) significantly accommodates the limitation by mass transfer often encountered in macro-reactors [33-35]. Furthermore, the redox reactions taking place on electrodes are intensified by bringing them very close to each other [35, 36]. While treating urban WWTPs effluents, their ionic conductivity (i.e., in average 1000 µS cm^{-1}) is apparently too low for conventional undivided reactor (d_{elec} between 1 and 4 cm) [37]. This low value of electrical conductivity limits the efficiency and applicability of EAOPs in various terms; firstly, the huge ohmic drop in-between electrodes requires an application of significantly larger operating currents thus inducing a larger overall power consumption [34, 37]. Secondly, the oxidation of pollutants will quickly be limited by mass transfer towards the electrodes, particularly for heterogeneous oxidation. Thus, the efficiency of pollutant degradation is critically impacted [38]. Thirdly, supporting electrolyte is added most of the time to promote the mass transfer of pollutants making the EAOPs less attracting as environmental-friendly processes. Fortunately, the use of microfluidic reactors would allow the treatment of reclaimed wastewater without the need for supporting electrolyte [37, 39]. As a consequence, microfluidic configuration would allow not only innate mass transfer enhancement, but also cut in operation cost. This paper aims to review the main influencing operating parameters responsible for the EAOPs efficiency, with an emphasis on engineering aspects for further development guidance at larger scales.

2. Influence of main operating parameters on EAOPs efficiency

2.1. Applied current density/electrode potential

Applied current density is a crucial parameter in the application of electrochemical process to degrade organic pollutants. It is also closely related to the electrode potential through the Butler-Volmer relation **[40]**, which is the driving force for direct and indirect oxidation and reduction reactions **[41]**. An optimal range of j_{app} was systematically noticed, depending on the type of EAOP **[29, 33, 38, 42]**, anode and cathode materials **[29, 38]**, on operating conditions (**Table 1**) as well as on the configuration mode of microfluidic reactors **[34, 37, 38]**. This apparent optimal value of j_{app} occurs due to two main reasons; either the electrical current is too low to produce significant quantity of oxidants or, on the contrary, too many electrical charges are given to the system till the redundant charges are wasted to unwanted side-reactions. Hence, the current efficiency (η, in %) is commonly written under the form given in **Eq. (1) [38]**.

$$\eta = 100\frac{n_e F C_{SOL} \dot{V}_F X}{j_{app} S} \quad (1)$$

where n_e is the number of required electrons for pollutant conversion, F is the Faraday constant (96,485 C mol^{-1}), $\dot{V}_F$ is the flow rate (in m^3 s^{-1}), X is the conversion rate, j_{app} in A m^{-2}, C_{SOL} is the initial pollutant concentration (in mol m^{-3}) and S is the electrode surface area (in m^2).

Figure 1 illustrates the percentages and η of chloroacetic acid removal by electro-oxidation (EO) at different current densities and flow rates. From **Fig. 1(a)**, it was observed that at low current density, organic abatement increased with applied current. The degradation was kinetically controlled by charge transfer and that was the reason why it increased with j_{app}, whereas in the region of high j_{app}, the percentage of abatement increased negligibly or remained constant with further increase in j_{app}. The degradation was kinetically controlled by organics mass transfer to the electrode. Excessive charge would be used for parasitic reactions. As a result, the η plot depicted a maximum where it

increased with further increase in j_{app} (**Fig. 1(b)**). Several other works have come up with similar deduction **[34, 37, 39, 43]**.

However, it is important to consider the matrices effects such as unwanted by-products formation as well as scaling phenomena (Section 2.6), when optimizing j_{app}. This has not been examined yet in microreactors application for wastewater treatment.

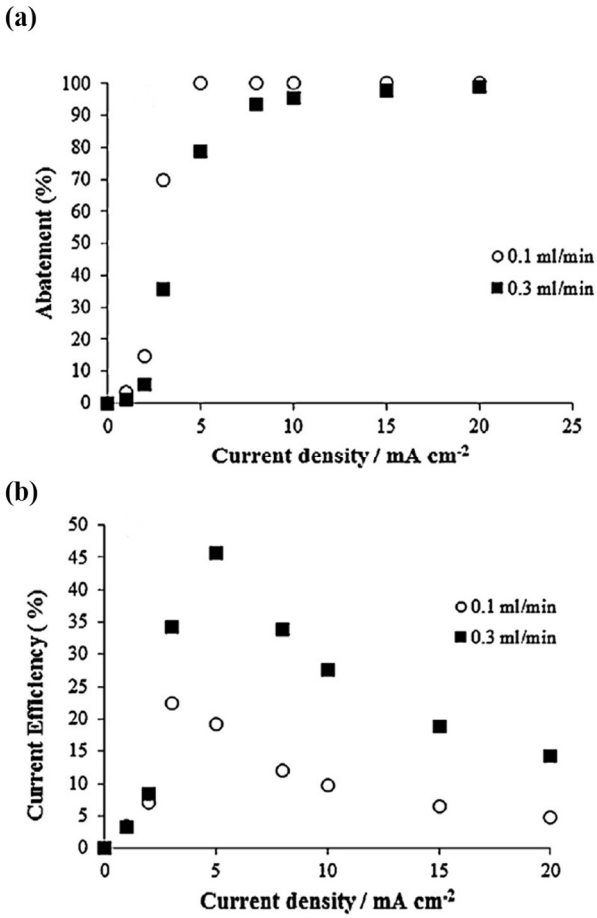

Fig. 1. **(a)** Percentage and **(b)** current efficiency (η) of degradation of chloroacetic acid during EO process in microfluidic reactor as a function of j_{app} at different flow rates. Initial pollutant concentration: 5 mM, d_{elec}: 50 µm, anode: BDD, cathode: stainless steel, surface area: 5 cm^2 (Adapted with permission from **[38]**. Copyright 2014, Elsevier).

2.2. Flow rate

The flow rate is an important parameter because it determines the residence time (τ) of the effluent to be treated in the electrolytic reactive zone. Generally, the influence of the flow rate depends on the electrochemical process occurring on electrode surfaces. According to **Fig. 1**, in the region where the process was kinetically controlled by charge transfer (lower j_{app}), organic removal was more efficient with lower flow rate. It was due to higher τ, thus there was a longer treatment of pollutant per charge applied. When the abatement of pollutant was controlled by mass transfer, the removal increased with the flow rate as a result of mass transfer intensification. η was also improved due to similar reasons (**Fig. 1**). Similar trend of conclusion has been documented in several works across literature **[29, 30, 33, 37-39]**.

2.3. Interelectrode distance

Despite being in micrometric conditions, the interelectrode distance (d_{elec}) between anode and cathode still plays a determining role towards the reaction mechanism occurring inside the microfluidic reactor. **Figure 2** plots the percentage of color and chemical oxygen demand (COD) removal during an electro-Fenton (EF) process to oxidize acid orange dye pollutant. The highest color (100%) (**Fig. 2(b)**) and COD (80%) (**Fig. 2(c)**) removals were achieved at lower d_{elec} (120 vs. 240 µm) at 20 A m^{-2} (2 mA cm^{-2}) **[42]**. It was attributed to higher H_2O_2 production (**Fig. 2(a)**) with smaller d_{elec} **[42]**. Lower distance resulted in a higher contribution of dissolved oxygen (O_2) formed on anode via **Eq. (2)** to produce H_2O_2 via **Eq. (3)**. Furthermore, the lower distance also led to a more uniform distribution of dissolved O_2 thus favoring H_2O_2 formation **[42]**. Adversely, further decreasing in d_{elec} led to lower residence time in the reactor. Thus, it led to lower accumulation of H_2O_2 and faster mass transfer of H_2O_2 towards the anode, before being oxidized back to dissolved O_2 (**Eq. (4)**).

$$2H_2O \rightarrow O_2 + 4H^+ + 4e^- \quad (2)$$

$$O_2 + 2H^+ + 2e^- \rightarrow H_2O_2 \quad (3)$$

$$H_2O_2 \rightarrow O_2 + 2H^+ + 2e^- \quad (4)$$

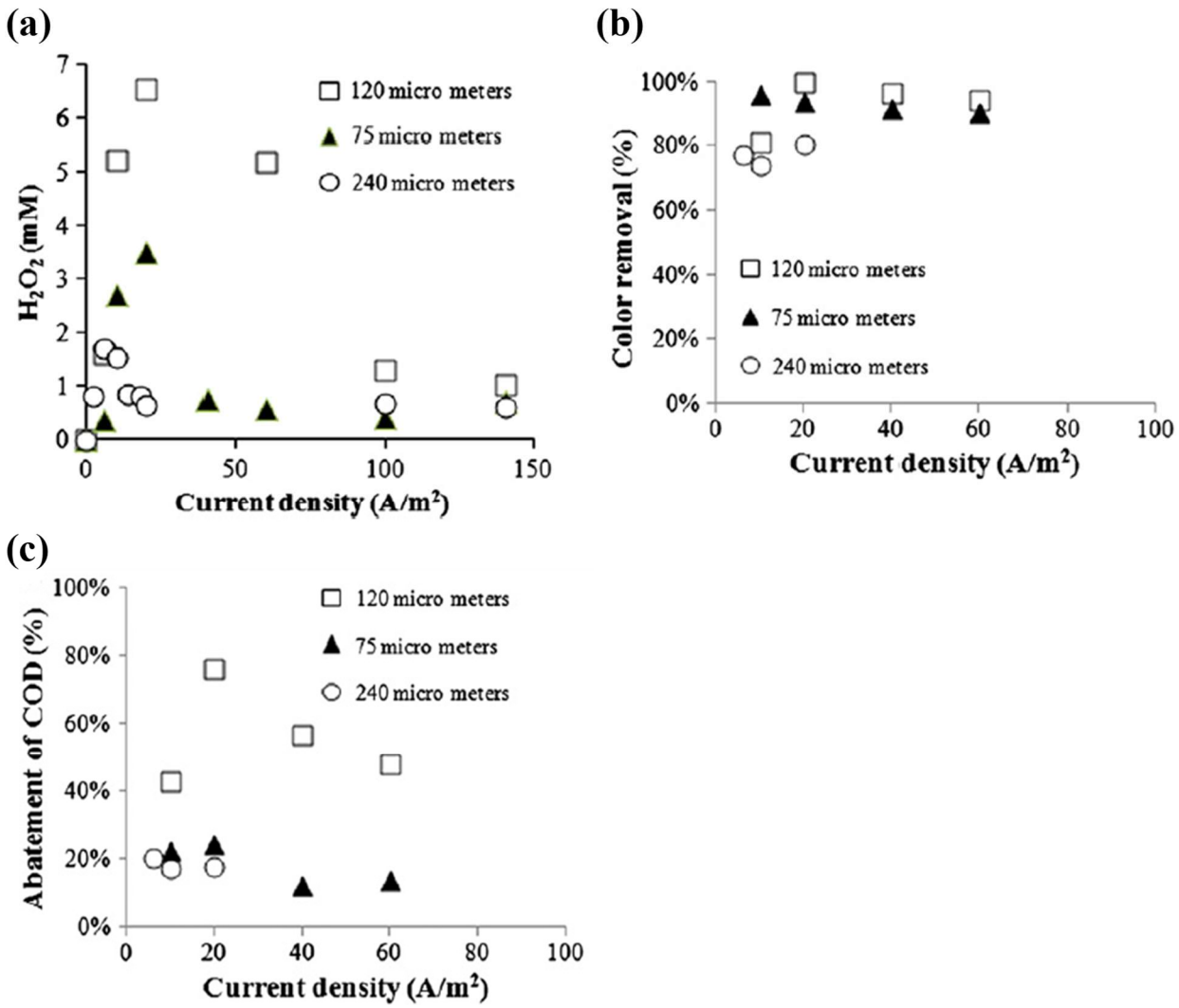

Fig. 2. **(a)** Hydrogen peroxide (H_2O_2), percentage of **(a)** color removal and **(b)** COD removal of organic dye using EF inside microfluidic reactor with different d_{elec} of 75, 120 and 240 µm at different j_{app}. Anode: IrO_2-Ta_2O_5/Ti, cathode: graphite. Initial dye concentration: 0.43 mM, Fe^{2+}: 0.5 mM (Adapted with permission from **[42]**. Copyright 2013, Elsevier).

When the interelectrode gap decreases, redox reactions on both anode and cathode are intensified. Mass transfer towards both electrodes is also significantly improved. This has been demonstrated

during the electro-oxidation of tetrachloroethane inside a microfluidic reactor operating using 50 and 75 µm d_{elec} [44]. Better abatement and η were noticed using lower d_{elec} and it was due to a better mass transfer of the pollutant towards the electrodes.

While progressively transitioning into the micrometric scale by reducing the interelectrode gap, the electrochemical cell voltage is reduced [37]. It occurs owing to the reduction of ohmic drop in-between electrodes. This phenomenon has clearly been presented in Fig. 3. It illustrates the variation of ohmic resistance ($\sum RI$) happening inside electrochemical reactors with large range of d_{elec} at different possible supporting electrolyte concentrations [34]. Considering for example the lowest supporting electrolyte (0.5 g L^{-1}), the $\sum RI$ measured inside stirred tank reactor with 25000 µm (2.5 cm) d_{elec} was 346 Ω. The resistance was reduced to 6 Ω inside a microfluidic reactor operating using similar 0.5 g L^{-1} supporting electrolyte.

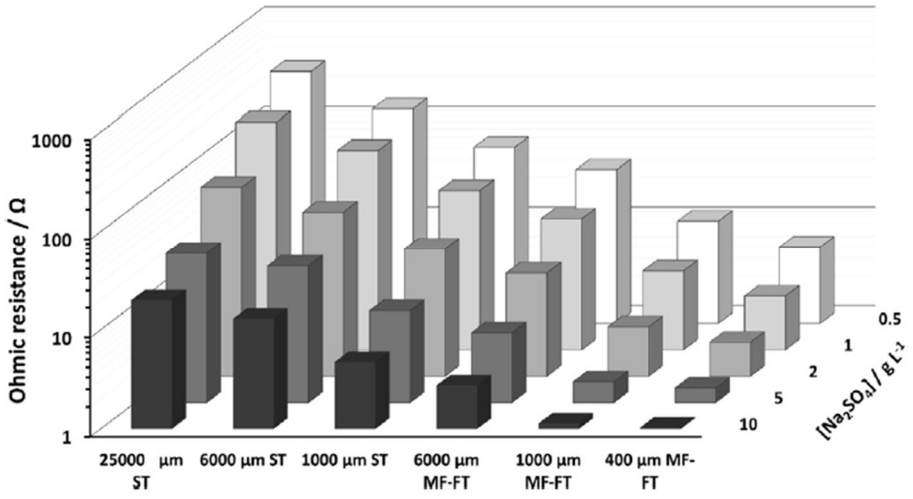

Fig. 3. Variation of ohmic resistance as a function of d_{elec} and different concentrations of supporting electrolyte (Adapted with permission from [34]. Copyright 2018, Elsevier).

In addition, there has been a study conducted by Khongton et al. in which the EO experiments were performed at different d_{elec} (250 to 750 µm), while keeping the τ constant [39]. For that, the flow rate was adjusted according to the d_{elec} to keep the residence time identical. This important feature should

be taken into account in articles, in order to have comparable hydrodynamics while varying d_{elec}. A similar approach has been adopted more recently with the investigation of larger range of d_{elec} (50 to 3000 µm) **[36, 45]**.

2.4. Electrode material

Depending upon the type of EAOP intended, electrode materials are selected accordingly. Advanced EO normally operates with anode possessing high overpotential for O_2 evolution such as lead oxide (PbO_2), tin oxide (SnO_2) and BDD (boron doped diamond), which possesses $E^0_{H_2O/O_2}$ of 1.8-2.0, 1.9-2.2 and 2.2-2.6 V/SHE respectively **[16]**. It allows the generation of potent oxidant such as $^{\bullet}OH$ on its surface via **Eq. (5)**.

$$M + H_2O \rightarrow M(^{\bullet}OH) + H^+ + e^- \quad (25)$$

BDD has received great attention due to its efficiency, stability, better life-span and high $E^0_{H_2O/O_2}$. These anodes are called non-active anodes, because the produced $^{\bullet}OH$ are loosely attached on anode surface by physisorption **[46]**. Hence, they can react quasi non-selectively with organic pollutants to oxidize them into simpler forms. When EO mode is solely intended, electrodes possessing high hydrogen (H_2) evolution potential (close to 0 V/SHE) such as stainless steel, platinum (Pt), titanium (Ti), nickel (Ni) or other metals are used **[22]**. Thus, H_2O_2 generation, which is as well an oxidant, is avoided.

When EF process is applied, cathode with low overpotential for H_2 evolution (towards negative potential values) is used. The most common cathodes are carbonaceous-based materials such as graphite, carbon sponge, activated carbon fiber, graphite felt and carbon felt **[16, 23]**. The purpose is

to generate H_2O_2 *in-situ* from O_2 reduction via **Eq. (3),** H_2O_2 being one of the reagents (with Fe^{2+}) of Fenton process provided in **Eq. (6)**.

$$Fe^{2+} + H_2O_2 \rightarrow Fe^{3+} + {\bullet}OH + OH^- \quad (6)$$

Furthermore, carbonaceous gas diffusion electrode has also been used to even improve H_2O_2 production by maximizing the contact between cathode, O_2 (by supplying air flow) and electrolyte **[16]**. An anode possessing low overpotential for O_2 evolution is used for EF, e.g., Pt, RuO_2 and/or IrO_2. These anodes are called active anodes, because $^{\bullet}$OH are strongly abided to the metal by chemisorption **[22]**. The metal M may form higher oxide MO and its decomposition releases O_2. On an active anode, water oxidation produces dissolved O_2 which is the precursor of H_2O_2 following **Eq. (2)**. Thus, the EF reagents are electrocatalytically regenerated (**Eqs. (3)** and **(7)**) in the electrolytic cell.

$$Fe^{3+} + e^- \rightarrow Fe^{2+} \quad (7)$$

A coupling of EAOP can be done in a single electrochemical cell simply by changing the electrode material. Successive attempts have been made in submillimetric reactor configuration for example during the degradation of chloroacetic acid **[38]** and Acid Orange 7 dye **[29]** by coupled EO-EF using BDD and compact graphite as anode and cathode respectively. A summary of different electrode materials used in EAOPs operated in microfluidic condition is given in **Table 1**. Changing the electrode material could give notable impact especially on overall operational cost, stability – thus durability of an EAOP and porosity – thus feasibility of the electrodes to adapt to a chosen reactor design. Overpotential of a specific electrochemical reaction might differ from one material to another, hence this phenomenon shall not be overlooked. Nonetheless, the simplicity to operate coupled electrochemical processes within a single reactor should further be exploited by researchers so that more advantages of EAOP could be unveiled: perhaps it could compete with other established technologies to treat wastewater.

2.5. Initial concentration of pollutant

The concentration of pollutant to be treated in the effluent can have an impact on the kinetics and efficiency of its degradation **[33]**. The results of EO of formic acid in a microfluidic reactor at varying formic acid concentrations, as plotted in **Fig. 4**, could explain the mechanism **[33]**. In the lower range of concentrations ($\leq$ 5 mmol L^{-1}), high pollutant oxidation was achieved and it was independent of applied current. The degradation process was supposed to be controlled by mass transfer. Contrastingly, using higher formic acid concentration ($\geq$ 15 mmol L^{-1}), a decrease of the degradation yield was noted but η increased (**Eq. (1)**). It suggested that the availability of pollutant near the anode surface was no longer the limiting factor, meaning that the kinetics was therefore limited by the charge transfer. Elsewhere, the degradation efficiency of organic dye was evaluated by either EO or EF process in microfluidic configurations **[30]**. Once again, lower organic abatement at higher concentration was observed but with drastic decrease in energy consumption (**Fig. 4(c)**). The latter was attributed to lower impact of parasitic oxidation reactions and therefore to the higher η.

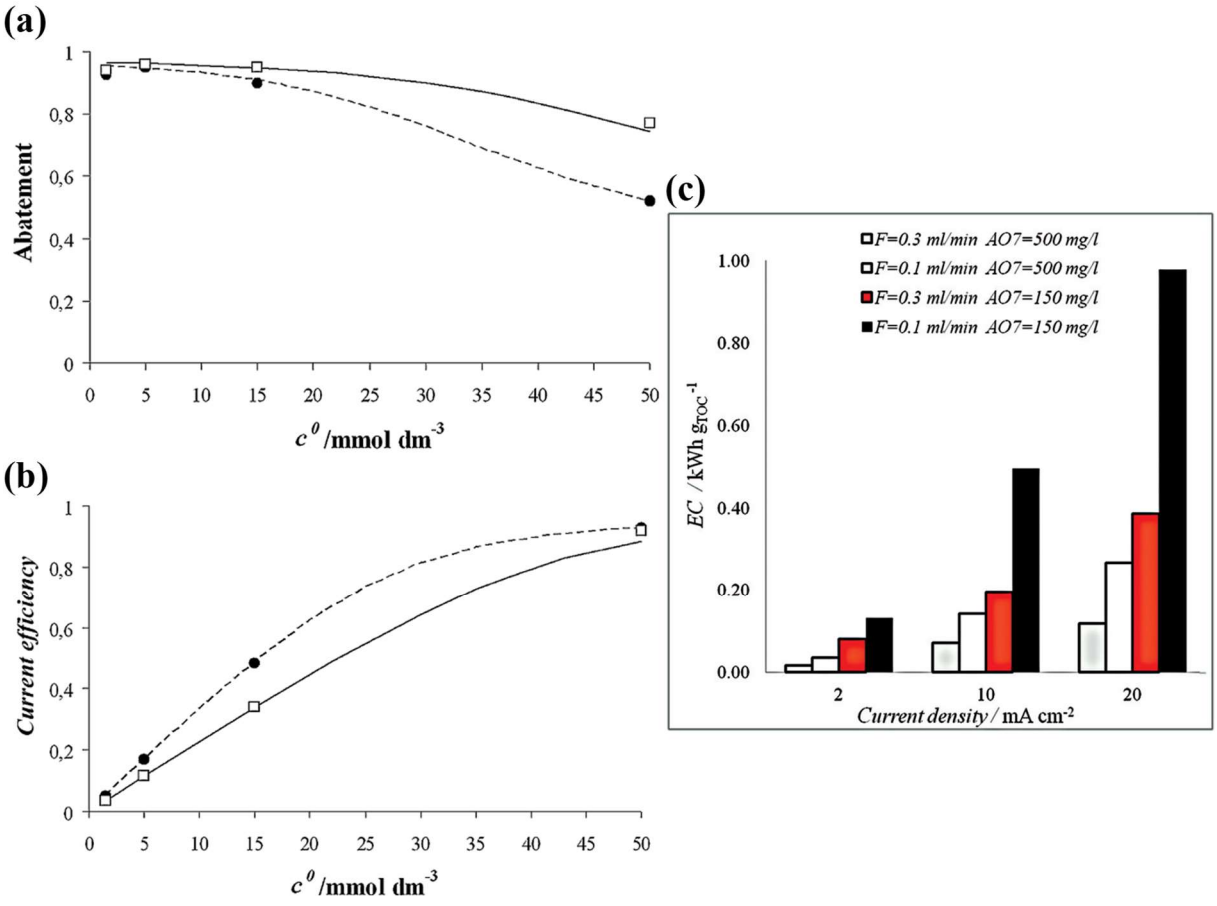

Fig. 4. Formic acid removal **(a)** using EO and the associated η values **(b)** at varying initial formic acid concentrations using 50 µm d_{elec} (adapted from Scialdone et al. **[33]**). (●): 6.7 and (□): 10 mA cm^{-2}. **(c)** Variation of specific power consumption during organic dye (acid orange 7 (AO7)) degradation at different dye concentrations and j_{app} using d_{elec} of 50 µm (Adapted from Sabatino et al. **[30]**. Copyright 2016, Wiley).

When high j_{app} was used to treat highly concentrated wastewater particularly using BDD as anode, the organic oxidation would be limited by mass transfer **[46]**. It is because sufficient electrical charge was supplied, which provided sufficient amount of $^{\bullet}OH$ to quickly and efficiently degrade the organics. **Figure 5** gives an example of such case where landfill leachate waste was electro-oxidized using different anodes at 2 A **[47]**. Consequently, organic degradation could be modeled using a pseudo first-order kinetic rate, when its oxidation was independent of initial organic content.

In real field applications, since the type of pollutant and its concentration vary correspondingly with the origin of waste effluent, attention should be given to the value of current intensity to be applied so that minimal charge would be gone to the targeted waste to minimize unnecessary energy consumption.

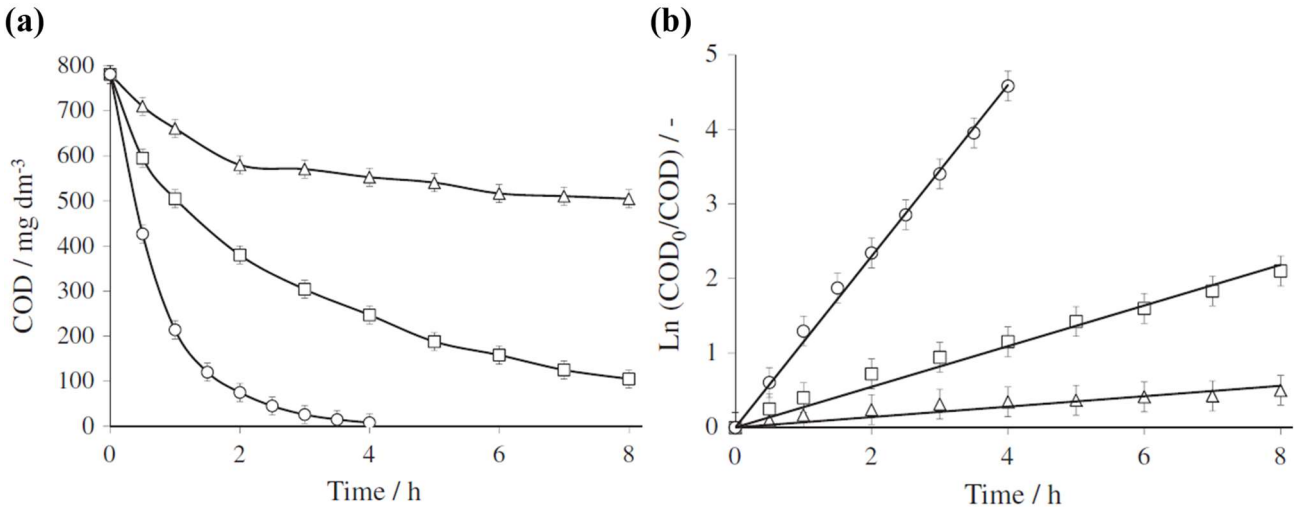

Fig. 5. **(a)** COD abatement and **(b)** pseudo first-order kinetic plot during the EO of landfill leachate wastewater using (△): $TiRuSnO_2$, (□): PbO_2 and (○): BDD anodes. *I*: 2 A and d_{elec}: 5000 µm (Adapted with permission from **[47]**. Copyright 2013, Elsevier).

2.6. Effluent matrices

To date, most of the investigations dealing with water treatment using microfluidic electrochemical cells reported in literature were carried out using synthetic solutions containing targeted pollutants to be treated (**Table 1**), such as organic acids **[33, 48]**, organochloride compounds **[38, 44, 49]**, organic dyes **[29, 30, 42, 50]** and herbicides **[32, 51, 52]**.

Amongst those published in literature, only few studies were done using real wastewater effluents **[37, 39, 43, 53]**. A real wastewater effluent, depending on its origin, is well known to contain complex matrix components. It is rich with organic matter be it volatile or not **[54, 55]**, cyclic and aromatic compounds **[56]**, unrecovered nutrients **[57, 58]** as well as organo-halogenic compounds **[59, 60]**.

It has also been widely known throughout literature that halogenic byproducts (particularly chlorine-based, due to its prevalence) were amongst the limiting factor for the EAOP at industrial scale. While applying a typical value of current density for an EAOP using a current generator, the subsequent applied potential on anode very often surpasses the standard potential of oxidation of chlorate (ClO_3^-) and perchlorate (ClO_4^-) **[59, 61, 62]**. They are the most stable oxidized forms of chlorinated byproducts whilst unfortunately being categorized as harmful byproducts **[62, 63]**. Knowing this fact, surprisingly enough, no attempt has yet been made to study the fate of halogenic byproducts during advanced electro-oxidation process performed using microfluidic reactor.

Apart from plausible evolution of noxious byproducts during the process, real effluents often contain suspended solids. Implementing thin film electrochemical reactors implies micrometric distances in-between electrodes. Thus, filtration would perhaps be necessary as pretreatment. Next, mineral scaling could present another issue during the application of EAOP. It could occur in the presence of magnesium (Mg^{2+}) and/or calcium (Ca^{2+}) and carbonates (HCO_3^-/CO_3^{2-}) in the effluent, which are omnipresent in various water and wastewater. The local alkalization on cathode originating from the reduction of dissolved oxygen (O_2) (**Eq. (8)**) and/or water (H_2O) (**Eq. (9)**) **[64-66]**, induces the electro-precipitation of deposits (e.g., $Mg(OH)_2$ (**Eq. (10)**), $CaCO_3$ (**Eq. (11)**)) that progressively passivate the electrode **[67-69]**.

$$O_2 + 2H_2O + 4e^- \rightarrow 4OH^- \quad (8)$$

$$2H_2O + 2e^- \rightarrow 2OH^- + H_2 \quad (9)$$

$$Mg^{2+} + 2OH^- \leftrightarrow Mg(OH)_2 \quad (10)$$

$$Ca^{2+} + CO_3^{2-} \leftrightarrow CaCO_3 \quad (11)$$

The role of d_{elec} on the formation of electro-precipitation taking place inside microreactors and in the presence of BDD anode has been investigated recently in details **[36, 45]**. Higher $CaCO_3$ electro-precipitation was found using shorted d_{elec} when similar current density was applied (4 mA cm^{-2})

(**Figs. 6(a)-6(b)**). It could be explained by the fact that when d_{elec} decreases at constant current density, the cathode potential increases and the anode potential diminishes along with the cell potential. Thus, at larger d_{elec} the lower cathode potential (into water reduction region) led to higher H_2 gas evolution that detached the precipitates on the cathode as schematized in **Fig. 7**.

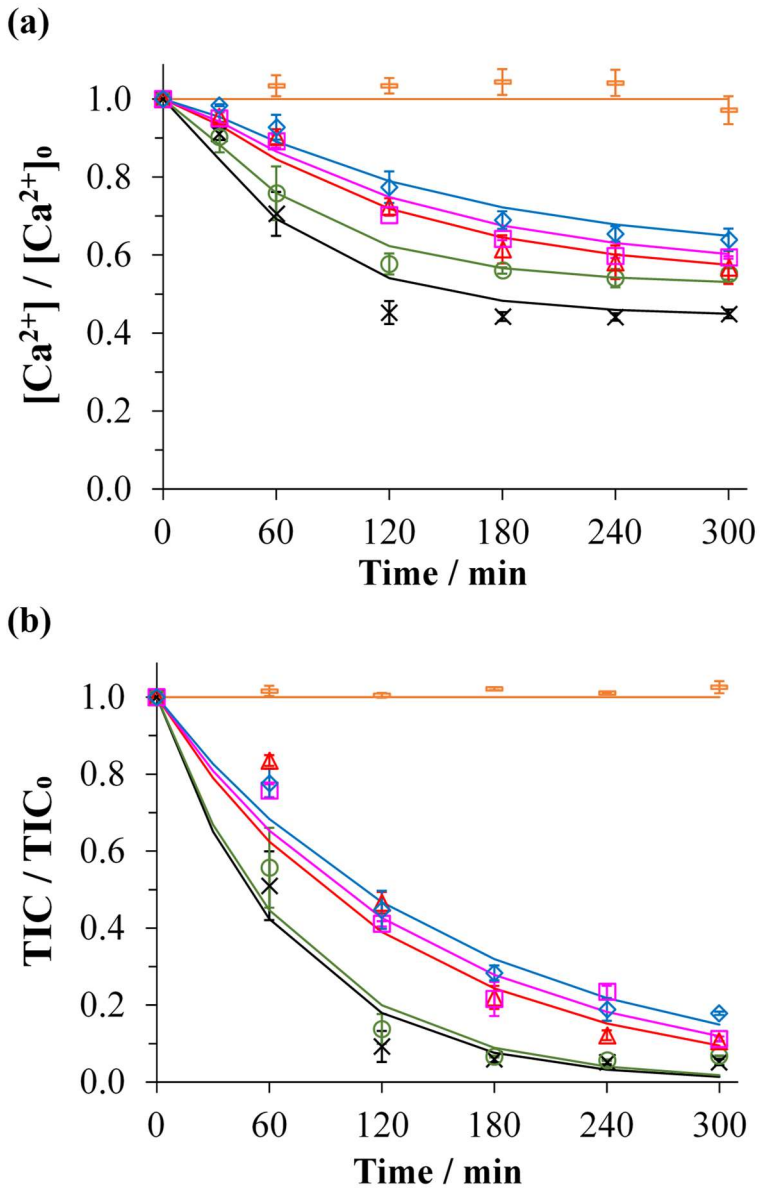

Fig. 6. Evolution of Ca^{2+} **(a)** and TIC **(b)** concentrations during the electrolysis at 4 mA cm^{-2} for different d_{elec} varying from micrometer range to millimeter range (—: 50 µm, ✕: 100 µm, ○: 250 µm, △: 500 µm, □: 1000 µm and ◇: 3000 µm). Cathode: SS and anode: BDD (Adapted with permission from **[36]**. Copyright 2021, Elsevier).

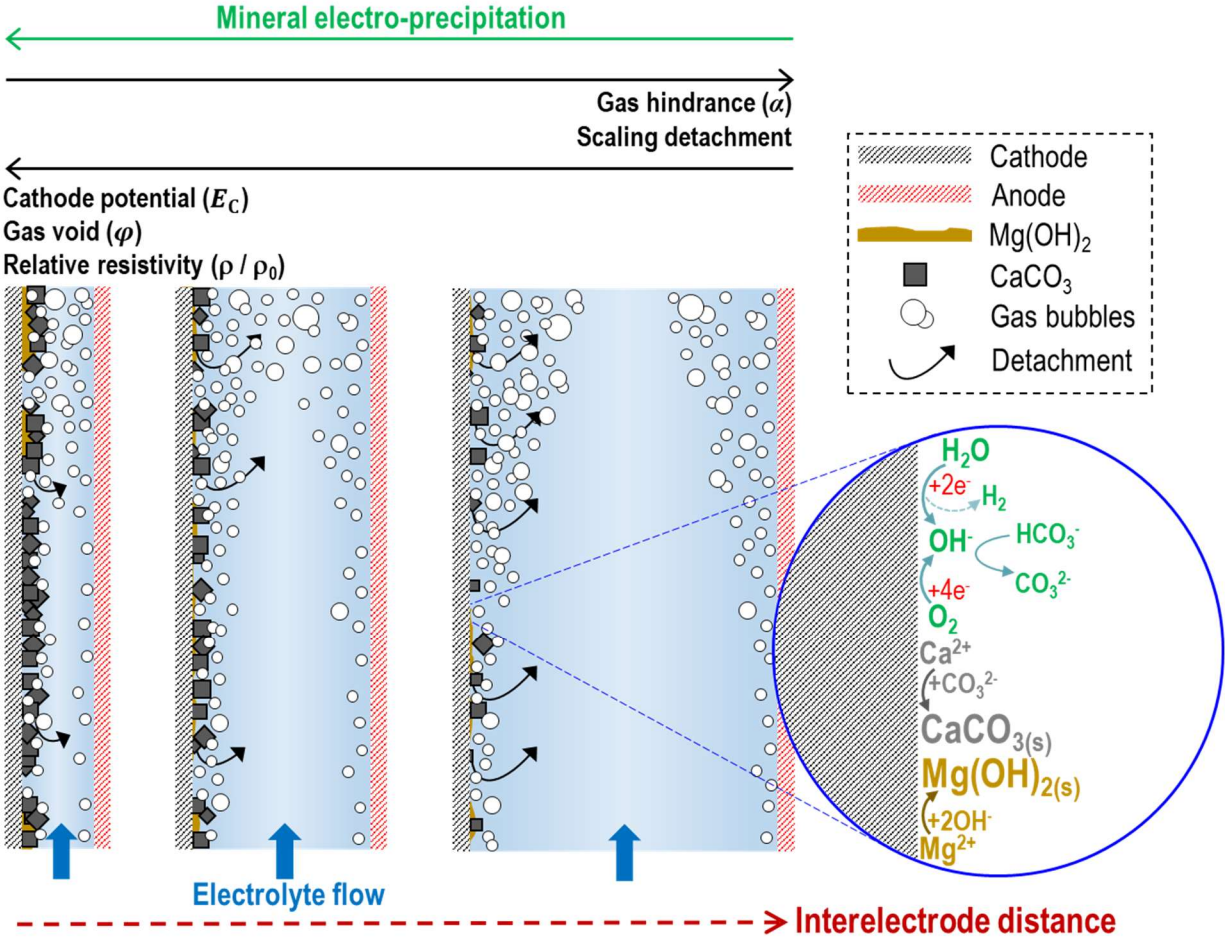

Fig. 7. Mechanistic scheme describing the influence of d_{elec} (100 - 3000 µm) and associated cathode potentials on the H_2 gas bubbles evolution and its impact on mineral electro-precipitation in the presence of precipitating ions (Ca^{2+}, HCO_3^-/CO_3^{2-}) (Adapted with permission from **[36]**. Copyright 2021, Elsevier).

Table 1. Literature review on the application of microfluidic reactors to treat wastewater.

Pollutant/matrix composition	EAOP	Mode	Electrode materials	d_{elec} / µm	Operating conditions	Ref
Oxalic acid	EO	Flow-by	Anode: BDD (9 cm^2) Cathode: Nickel (9 cm^2)	50, 360 and 750	Oxalic acid: 0.36 – 0.9 g L^{-1} j_{app}: 4.44 – 1.67 mA cm^{-2} (40 – 150 mA) Flow rate: 0.5 mL min^{-1}, Na_2SO_4: 0 or 5 g L^{-1}, pH: 2	[48]
Formic acid	EO	Flow-by	Anode: BDD (2.7 cm^2) Cathode: Nickel (2.7 cm^2)	50 and 75	Formic acid: 0.069 – 2.3 g L^{-1} j_{app}: 2.2 – 40 mA cm^{-2} (6 – 108 mA) Flow rate: 0.05 – 0.30 mL min^{-1}, pH: 2	[33]
Acid Orange 7	EF	Flow-by	Anode: Ti/IrO_2-Ta_2O_5 (5 cm^2) Cathode: Compact graphite (5 cm^2) or Carbon felt (5 – 6 cm^2)	7, 120 and 240	Acid Orange 7: 0.15 g L^{-1} j_{app}: 1 – 15 mA/cm^2 (5 – 75 mA) Flow rate: 0.1 mL min^{-1}, Na_2SO_4: 5 g L^{-1}, Fe^{2+}: 0.076 g L^{-1}, volume: 50 mL	[42]
Chloroacetic acid	EO EF EO-EF	Flow-by	**EO**: Anode: BDD, Cathode: Stainless steel **EF**: Anode: Ti/IrO_2-Ta_2O_5, Cathode: Compact graphite **EO-EF**: Anode: BDD, Cathode: Compact graphite All electrode surface area: 5 cm^2	50 and 100	Chloroacetic acid: 0.473 g L^{-1} j_{app}: 1 – 20 mA cm^{-2} (5 – 100 mA) Flow rate: 0.1 – 0.6 mL min^{-1}, EF: 0 or 0.076 g L^{-1} Fe^{2+}, pH: 3 (EF)	[38]
Acid Orange 7	EO EF Indirect oxidation by active chlorine (IOAC)	Flow-by	**EO**: Anode: BDD, Cathode: Nickel **EF**: Anode: Ti/IrO_2-Ta_2O_5, Cathode: Compact graphite **IOAC**: Anode: Ti/IrO_2-Ta_2O_5, Cathode: Nickel All electrode surface area: 5 cm^2	50, 75, 120 and 240	Acid Orange 7: 0.15 g L^{-1} j_{app}: 2 – 14 mA cm^{-2} (10 – 70 mA) Flow rate: 0.1 – 0.4 mL min^{-1}, EF: 0.034 – 0.152 g L^{-1} Fe^{2+}, IOAC: 0.993 g L^{-1} NaCl, pH: 7 (EO, IOAC) and 3 (EF)	[29]

Pollutant/matrix composition	EAOP	Mode	Electrode materials	d_{elec} / µm	Operating conditions	Ref
Tetrachloroethane	EO ER EO-ER	Flow-by	**EO**: Anode: BDD, Cathode: Nickel **ER**: Anode: DSA, Cathode: Silver **EO-ER**: Anode: BDD, Cathode: Silver All electrode surface area: 3-4 cm^2	50 and 75	Tetrachloroethane: 0.151 – 0.285 g L^{-1} j_{app}: 3 – 15 mA cm^{-2} (9 – 45 mA) Flow rate: 0.1 – 0.4 mL min^{-1}, pH: 2	[44]
Dichloroacetic acid	ER	Flow-by	Anode: Ti/IrO_2-Ta_2O_5, Cathode: Compact graphite **Configuration in series**: Surface area: 4 cm^2 (each electrode) **Configuration in stack**: Surface area: 6 cm^2 (each chamber)	100	Dichloroacetic acid: 0.013 – 0.0645 g L^{-1} j_{app}: 10 – 48 mA cm^{-2} Flow rate: 0.05, 0.1 and 0.2 mL min^{-1}	[49]
Acid Orange 7	EO EF EF-EO	Flow-by	**EO**: Anode: BDD, Cathode: Nickel **EF**: Anode: DSA, Cathode: Graphite Configuration: single, 3 in series or in series with between 2 EAOPs All electrode surface area: 4 cm^2	EO: 50 EF: 120	Acid Orange 7: 0.15 and 0.5 g L^{-1} **EO**: j_{app}: 2 – 20 mA cm^{-2} Flow rate: 0.1 – 0.3 mL min^{-1} **EF**: j_{app}: 1 – 20 mA cm^{-2} Flow rate: 0.1 mL min^{-1}, Fe^{2+}: 0.076 g L^{-1}, pH: 3	[30]
Total organic carbon in reclaimed industrial WWTP effluent	EO	Flow-by	Anode: BDD (3.75 cm^2) Cathode: Nickel (3.75 cm^2)	50	TOC_0: 0.21 g L^{-1} j_{app}: 5.3 – 53.3 mA cm^{-2} (20 – 200 mA) Flow rate: 0.1 – 0.5 mL min^{-1}, pH: 6.2, volume: 0.05 L	[37]
Diuron herbicide	EO	Flow-by	Anode: Graphite sheet (3 cm^2) Cathode: Stainless steel (3 cm^2)	250 – 750	Diuron: 0.01 g L^{-1} j_{app}: 0.16 – 0.64 mA cm^{-2} (0.5 – 2 mA) pH: 3 – 10, conductivity: 6.7 – 1000 µS cm^{-1}	[39]
Paracetamol in synthetic solution and reclaimed municipal WWTP effluent	EO	Flow-by	Anode: BDD (50 cm^2) Cathode: Carbon felt (50 cm^2)	50 – 1000	Paracetamol: 0.015 g L^{-1} j_{app}: 2 to 12 mA cm^{-2} pH: 3 or neutral, Na_2SO_4: 0.14, 0.57 and 1.42 g L^{-1}, conductivity: 230 – 2000 µS cm^{-1}, flow rate: 430 mL min^{-1}, volume: 0.2 or 0.5 L	[53]

Pollutant/matrix composition	EAOP	Mode	Electrode materials	d_{elec} / µm	Operating conditions	Ref
Synthetic solution containing magnesium, calcium, carbonates	EO	Flow-by	Anode: BDD (50 cm^2) Cathode: Stainless steel (50 cm^2)	500	Magnesium: 0.005 g L^{-1}, calcium: 0.15 g L^{-1}, total inorganic carbon: 0.06 g-C L^{-1} j_{app}: 0.4 to 4 mA cm^{-2} pH: 7.6, conductivity: 1000 µS cm^{-1}, flow rate: 100 mL min^{-1}, volume: 0.5 L	[45]
Synthetic solution containing magnesium, calcium, carbonates	EO	Flow-by	Anode: BDD (50 cm^2) Cathode: Stainless steel (50 cm^2)	50 – 3000	Magnesium: 0.005 g L^{-1}, calcium: 0.15 g L^{-1}, total inorganic carbon: 0.06 g-C L^{-1} j_{app}: 4 mA cm^{-2} pH: 7.6, conductivity: 1000 µS cm^{-1}, flow rate: 10 - 600 mL min^{-1} (adapted to d_{elec}), volume: 0.5 L	[36]
Mordant Orange dye	EO	Flow-through	Anode: BDD mesh (25 cm^2) Cathode: Ti/RuO_2 mesh (26 cm^2)	150	Dye: 0.1 g L^{-1}, j_{app}: 10 – 40 mA cm^{-2} (250 – 1000 mA), pH: 6.2 – 6.6, conductivity: 11 µS cm^{-1} – 108 mS cm^{-1} (in Na_2SO_4 and NaCl), rotation speed: 200 – 1000 rpm, volume: 0.3 L	[50]
Paracetamol in synthetic solution	EO	Flow-through	Anode: Perforated BDD (14 cm^2) Cathode: Carbon felt (14 cm^2)	500	Paracetamol: 0.015 g L^{-1} j_{app}: 4 mA cm^{-2} Na_2SO_4: 0.57 g L^{-1}, pH: neutral, conductivity: 850 µS cm^{-1}, volume: 4 L	[70]
Clopyralid in simulated soil washing effluent	EO	Flow-through	Anode: BDD mesh (33 cm^2) Cathode: Perforated plate stainless steel (33 cm^2)	400	Clopyralid: 0.1 g L^{-1} j_{app}: 10 mA cm^{-2} Flow rate: 1670 mL min^{-1}, volume: 1 L	[32]
Clopyralid in simulated soil washing effluent	EO	Flow-through	Anode: BDD (50 cm^2) or Ti/RuO_2-IrO_2 MMO mesh (53 cm^2) Cathode: Perforated stainless steel plate (33 cm^2)	400	Clopyralid: 0.1 g L^{-1} j_{app}: 10 and 100 mA cm^{-2} Flow rate: 1670 mL min^{-1}, volume: 1 L	[34]
Clopyralid in simulated soil washing effluent	EF	Flow-through	Anode: Ti/RuO_2-IrO_2 MMO (53 cm^2) or BDD mesh (50 cm^2) Cathode: CB/PTFE-RVC or CB/PTFE-Al (33 cm^2)	400	Clopyralid: 0.1 g L^{-1} j_{app}: 20, 30 and 50 mA cm^{-3} Flow rate: 1170 mL min^{-1}, Fe^{2+}: 0.028 and 0.112 g L^{-1}, Na_2SO_4: 1 or 7.1 g L^{-1}, pH: 3, volume: 0.750 L	[51]

Pollutant/matrix composition	EAOP	Mode	Electrode materials	d_{elec} / µm	Operating conditions	Ref
Clopyralid in simulated soil washing effluent	EF	Flow-through	Anode: Ti/RuO_2-IrO_2 MMO (33 cm^2) Cathode: CB/PTFE-Al foam (33 cm^2), Al foam thickness: 5 mm. For scale-up study: 10 and 15 mm	150	Clopyralid: 0.1 g L^{-1} j_{app}: 10 – 60 mA cm^{-3} Flow rate: 2670 mL min^{-1}, Na_2SO_4: 7.1 g L^{-1}, volume: 2.25 L, pressurized air: 6 bars	[52]
Pretreated soil washing wastewater containing clopyralid herbicide	EO EF	Flow-through	**EO**: Anode: BDD mesh, Cathode: perforated stainless steel plate **EF**: Anode: BDD mesh, Cathode: CB/PTFE-Al foam All electrode surface area: 33 cm^2	150	400 g of soil polluted with 100 g kg^{-1} of clopyralid washed with 1 L water j_{app}: 10 – 100 mA cm^{-2} Flow rate: 400 – 1600 mL min^{-1}, EF: 0.028 g L^{-1} Fe^{2+}, pH: 3 (EF)	[43]

Abbreviations: EO: Electro-oxidation, ER: electro-reduction, EF: electro-Fenton, BDD: boron-doped diamond, DSA: dimensionally stable anode, CB: carbon black, PTFE: polytetrafluoroethylene, RVC: reticulated vitreous carbon, Al: aluminum, d_{elec}: interelectrode distance, j_{app}: applied current density, TOC: total organic carbon.

3. Design and modularity of microfluidic electrochemical cell

3.1. Mass transfer in submillimetric electrochemical reactors

The application of submillimetric reactor configurations requires further in-depth understanding regarding the mass transfer phenomenon at the core of the electrochemical cell. Thin film reactors **[71-73]** introduced in the early 80s consisted of a plate electrode (i.e., the working electrode (WE)) most of the time positioned horizontally and were equipped with a counter electrode at the downstream of the reactor (**Fig. 8(a)**). The reference electrode (RE) was positioned close to the WE, upstream if a 3-electrode configuration was adopted **[73]**. This thin film setup is not appropriate to receive wastewater effluent. Flow-by filter-press or flow-through reactor designs are more apt for wastewater applications at pilot or even industrial scale (e.g., **Figs. 8(b)-(c)**).

Sherwood (*Sh*) correlation (**Eq. (12)**) assuming Lévêque approximation is common in parallel-plate electrochemical reactors in the literature:

$$Sh = aRe^{b}Sc^{c}Le^{d} \quad (12)$$

where *Re* is the Reynolds number, *Sc* is the Schmidt number, *Le* is the dimensionless distance, *a*, *b*, *c* and *d* defined constant parameters.

It allows a dimensionless expression of the mass transfer coefficient (k_m) with dimensionless fluid properties as well as dimensionless reactor configurations under respective hydrodynamic regime of liquid flow. As a result, the extrapolation of k_m for a given reactor dimension during a scale up or scale down is possible.

Recently, it has been established for the first time a correlation between k_m and d_{elec} for a wide range of distance from microfluidic condition (100 µm) to millimetric configuration in a flow-by parallel-plate cell (**Fig. 9**) **[35]**. This should be beneficial not only to the application in environmental field but also in other electrochemistry areas. It allows a convenient estimation of k_m for a scale up or scale

down of an electrochemical reactor operated in comparable hydrodynamic regime. It further highlights the drastic increase of mass transfer as soon as d_{elec} is below 1 mm, which could be defined as the limit between microfluidic and macrometric behavior. Moreover, since the associated average *Sh* number (Sh_{ave}) as a function of d_{elec} is expressed in dimensionless form (**Fig. 9**) **[35]**, the correlation remains valid to other microfluidic reactor geometries of interest.

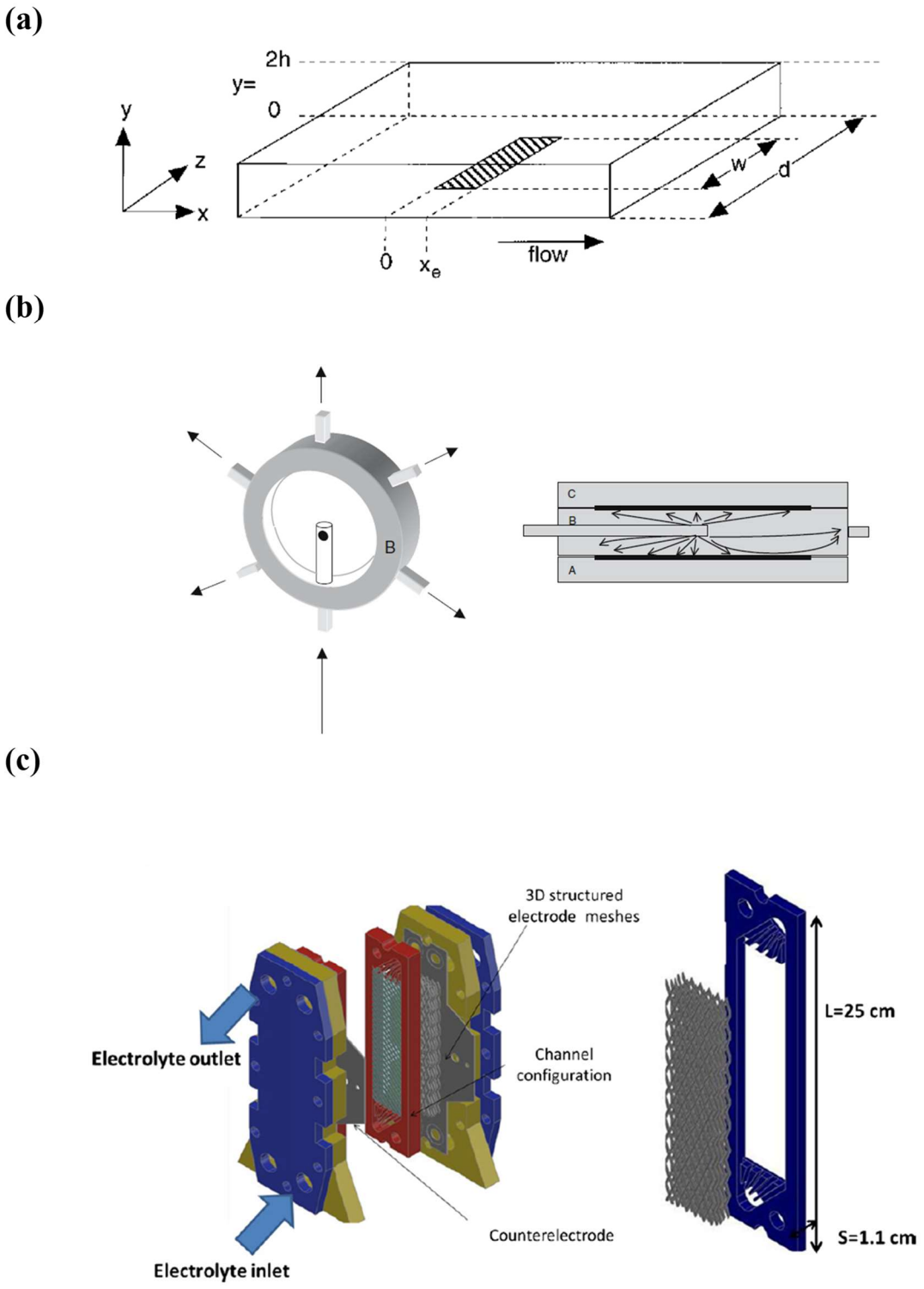

329

330 **Fig. 8**. **(a)** Thin-film channel flow cell reproduced from Cooper et al. **[73]** and more recent parallel-
331 plate electrochemical reactors such as **(b)** parallel-plate with impinging inlet (Reproduced with
332 permission from **[74]**. Copyright 2005, Elsevier) and **(c)** commercial parallel-plate filter-press type
333 reactor (Reproduced with permission from **[75]**. Copyright 2012, Elsevier).

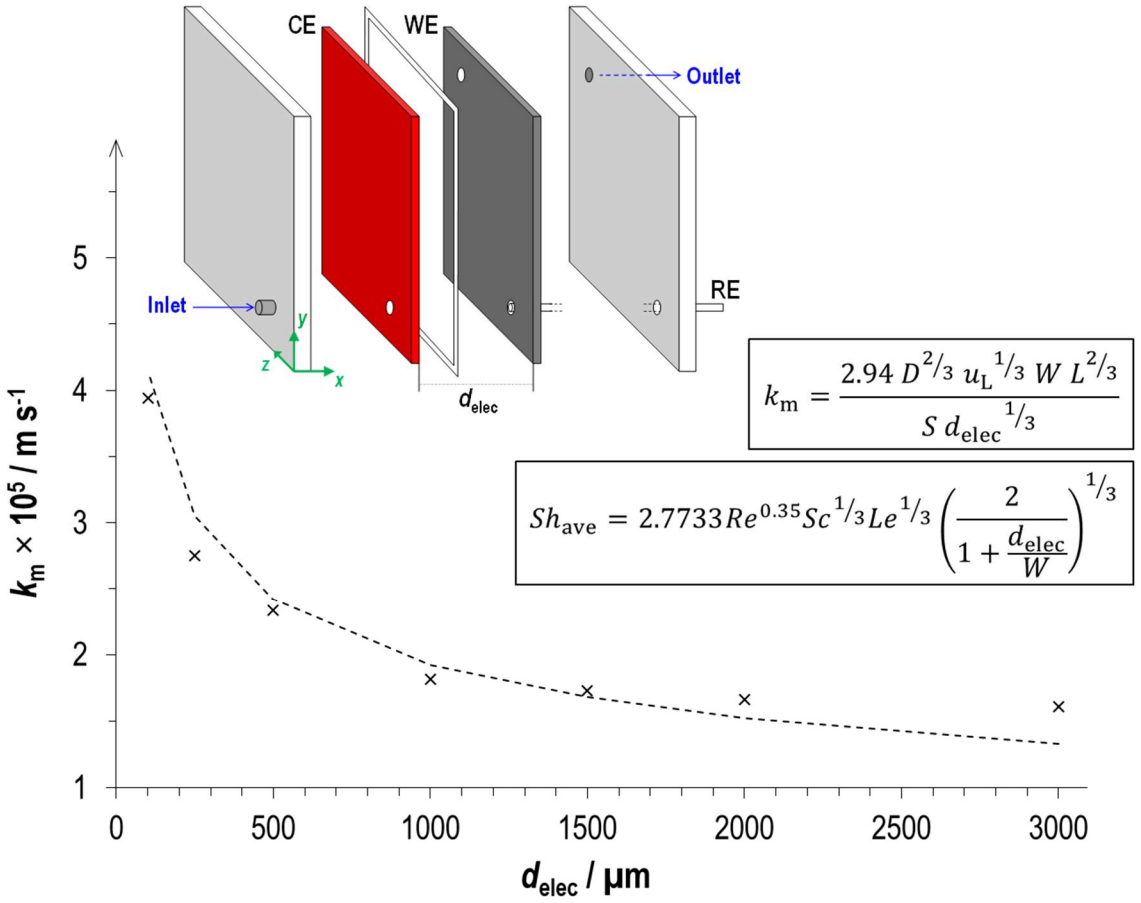

Fig. 9. Variation of experimental and theoretical average k_m as function of d_{elec} in a flow-by parallel-plate cell. Operating conditions: temperature: 25 °C, identical cross-sectional electrolyte velocity (u_L): 4 m min^{-1} and electrolyte residence time (τ): 0.025 min. W: electrode width (m), D_L: diffusion coefficient (m^2 s^{-1}), L: electrode length (m), S: effective surface area of working electrode (m^2) (Adapted with permission from **[35]**. Copyright 2021, Elsevier).

3.2. Microfluidic electrochemical reactor in wastewater treatment applications

To date, two electrochemical reactor designs have been proposed to treat wastewater in microfluidic conditions as summarized in **Table 1**. The first one is a flow-by design and the other one is a flow-through configuration as illustrated in **Fig. 10**.

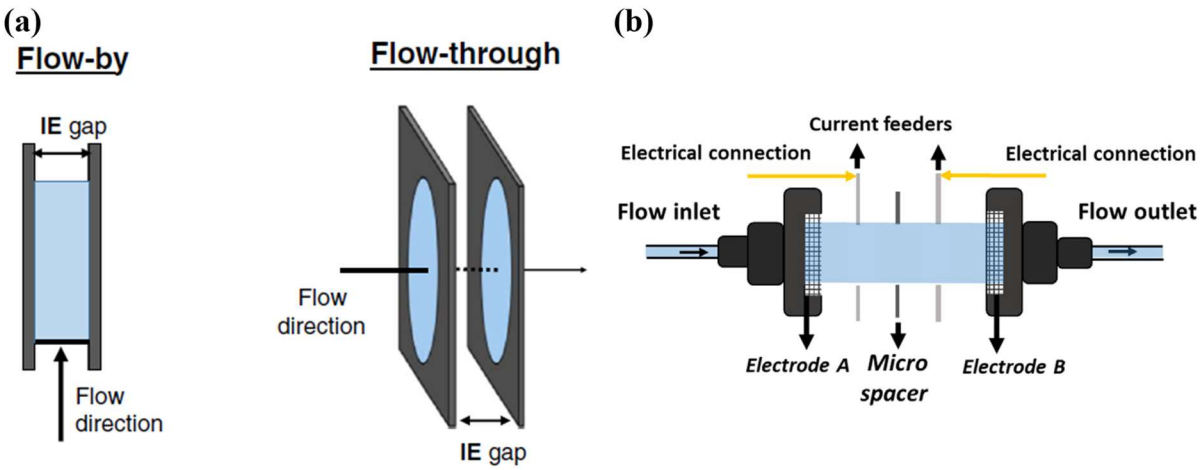

Fig. 10. **(a)** Difference between flow-by and flow-through electrolytic flow and **(b)** scheme of flow-through microfluidic cell (Adapted with permission from **[32]**. Copyright 2017, Elsevier).

In the flow-by configuration, the electrolyte flowed in between two planar electrodes separated by a micrometric distance **[32]**. In the flow-through mode, the electrodes were porous, typically meshes, which allowed the electrolyte to pass through them **[32]**. The two meshes of anode and cathode were separated by a spacer, micrometric in thickness, which gave microfluidic characteristics to the reactor **[32]**.

A comparison in terms of pollutant degradation as well as economic performance between the two designs has been performed and it has been illustrated in **Fig. 11**. It can be observed that both degradation of clopyralid and mineralization of total organic carbon (TOC) were faster using flow-through mode at both applied current investigated (**Figs. 11(a)-11(b)**). At 10 mA cm^{-2}, complete removal of clopyralid and TOC were obtained after 10.1 and 11.4 Ah dm^{-3} respectively using flow-

by mode, whilst they required 2.4 and 2.7 Ah dm^{-3} in flow-through mode. Lower E_{SP} was also obtained in the flow-through configuration, which was evaluated at 12 kWh m^{-3} using 10 mA cm^{-2} against 61 kWh m^{-3} in flow-by mode working at similar j_{app}. Better energetic performance was attributed not only to lower cell voltage but also to improved mass transfer [32, 34]. With 3-dimensional mesh electrodes in flow-through cell, higher geometric area and specific surface of electrode could be achieved over planar electrodes and more local turbulence occurred in the mesh. Therefore, the reactor design was more compact and k_m was higher compared to the flow-by design.

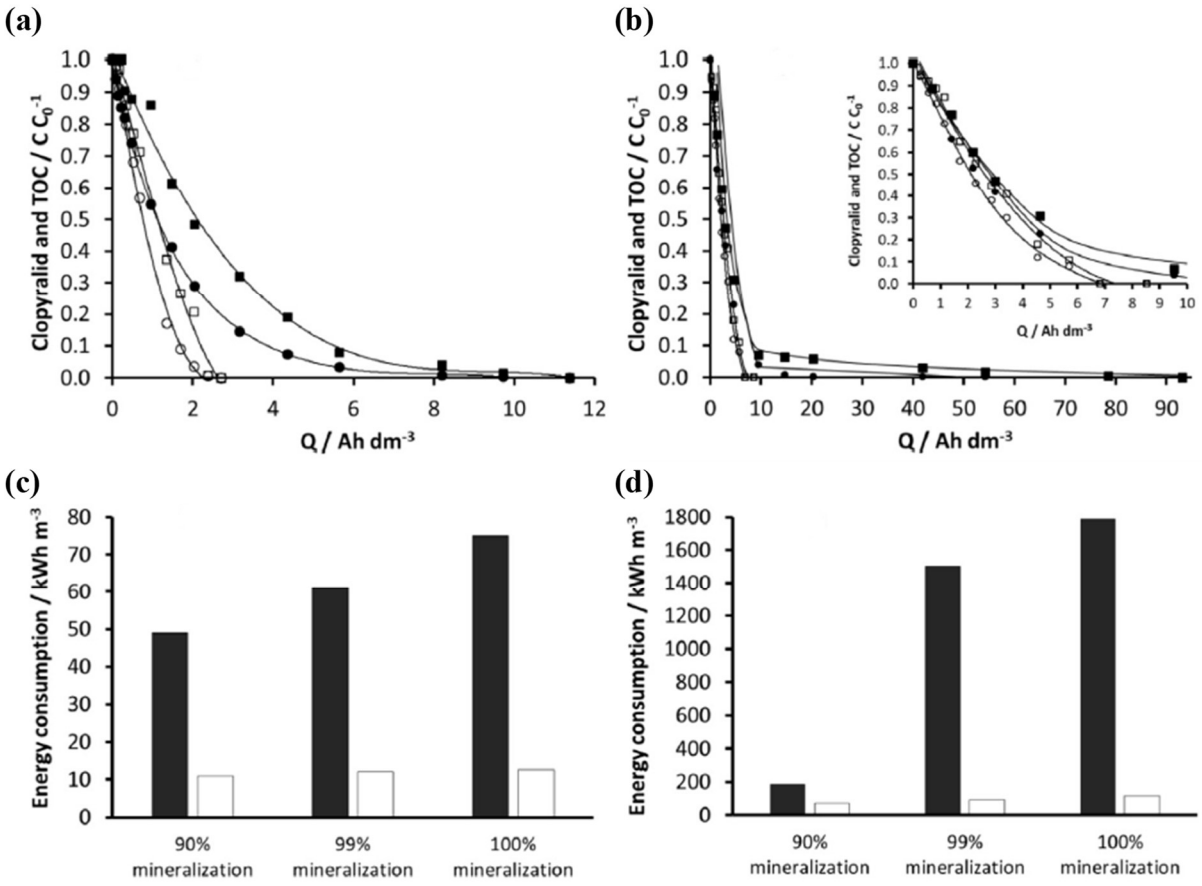

Fig. 11. Comparison of clopyralid pesticide (●, ○) and total organic carbon (TOC) (■, □) removal using flow-by (●, ■) and flow-through (○, □) microfluidic reactors by applying 10 (**(a)**, **(c)**) and 100 (**(b)**, **(d)**) mA cm^{-2}. Power consumption of flow-by (black bar) and flow-through (white bar) during the process to reach different mineralization degrees at 10 mA cm^{-2} **(c)** and 100 mA cm^{-}

372 [2] **(d)**. Flow-by d_{elec}: 3000 µm and flow-through d_{elec}: 400 µm. Anode: BDD and cathode: stainless
373 steel. (Adapted with permission from **[34]**. Copyright 2018, Elsevier).

374

375 Due to the fact that the electrochemical microreactor implies small volume within the cell, the
376 productivity of the process using such reactor design is often questionable. To address this problem,
377 several authors have tempted operating the reactors in series. For example, up to three flow-by
378 microfluidic reactors were operated in series (**Fig. 12(a)**) to degrade an organic dye up to 500 mg L^{-1}
379 [1] in concentration **[30]**. The results are presented in **Fig. 13**. It was shown that color and organics
380 removal as well as treatment productivity could effectively be improved by operating the cells in
381 series as expected. A coupling of two microfluidic reactors combining EF and EO were as well
382 modulated. The first process of EF was aimed to reduce organic content using cheap electrodes while
383 using low energy consumption, whilst from the second EO process, the strong oxidation by $^{\bullet}OH$ was
384 intended to achieve total organics degradation. Optimal coupling was obtained by adapting different
385 applied parameters required by each operation **[30]**. An assay has also been made to increase H_2O_2
386 production in a flow-through microfluidic cell **[52]**. It was done by using thicker cathode materials
387 (5, 10 and 15 mm in length, which gave 16.5 to 49.5 cm^3 in volume (depicted in **Fig. 12(b)**)) hence
388 sizing up the geometrical volume of electrochemical reactor. The authors reported having a
389 proportional increase in H_2O_2 production rate with the increasing cathode thickness. However, ohmic
390 resistance was reported to increase slightly when the thickness of cathode was increased. Cell voltage
391 also increased with electrode thickness. As a result, higher cell voltage entailed an increase in E_{SP}.

(a)

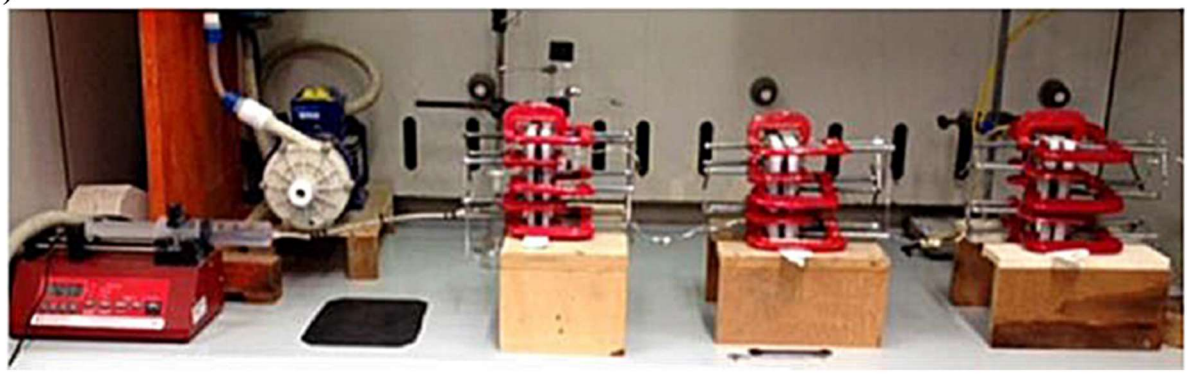

(b)

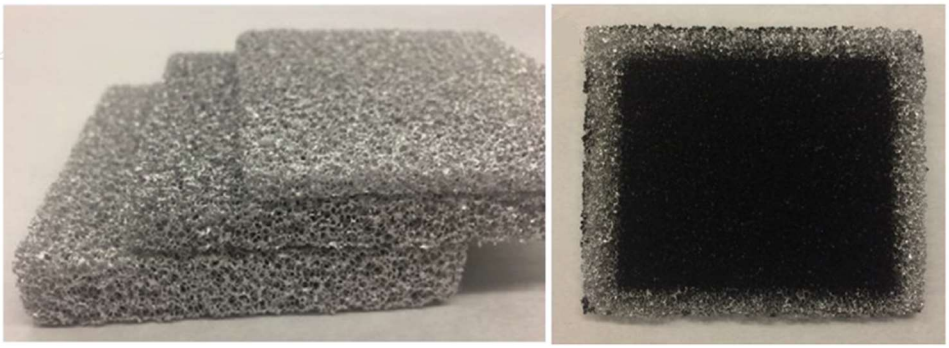

392

393 **Fig. 12**. **(a)** Flow-by microfluidic reactors operating in series (Reproduced with permission from
394 **[30]**. Copyright 2016, Wiley) and **(b)** cathode material thicknesses used in flow-through
395 microfluidic cell (Reproduced with permission from **[52]**. Copyright 2019, Elsevier).

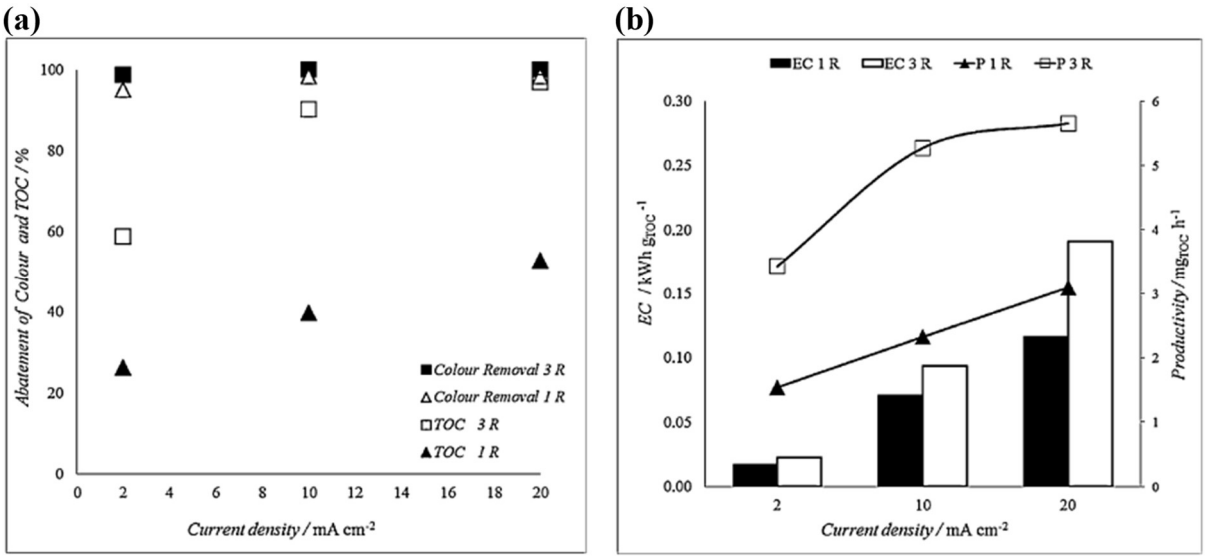

396

397 **Fig. 13**. **(a)** Color and TOC removal as well as **(b)** energy consumption and productivity for flow-
398 by microfluidic reactor working in single or in series at different j_{app} (Adapted with permission from
399 **[30]**. Copyright 2016, Wiley).

400

401 Recently, another innovative microreactor design has been introduced, which could be particularly
402 applicable in the field of wastewater treatment **[70]**. The reactor is illustrated in **Fig. 14**. This design
403 was proposed to reduce the mass transfer limitation often encountered in conventional macroreactors
404 as well as to address the low treatment capacity and the clogging issue related to microfluidic reactors.
405 It has been called reactive electro-mixing reactor and it consists of impellers, which themselves are
406 composed of thin film electrochemical reactors. The reactors were set on motion with the rotation of
407 the reactive electro-blades. One reactor can accommodate several impellers, which thus means
408 several microreactors in one macroreactor. In the meanwhile, the macroreactors could be operated in
409 series to increase significantly the productivity. Following on this way, a recent article reports on a
410 rotating electrochemical cell design with one electro-blade in rotation using BDD mesh as anode and
411 Ti/RuO_2 mesh as cathode, while combining electrooxidation with ultrasound **[50]**. The use of a solid

polymer electrolyte with 150 µm of thickness allowed operating with very low-conductivity solutions (10^{-5} S cm^{-1}).

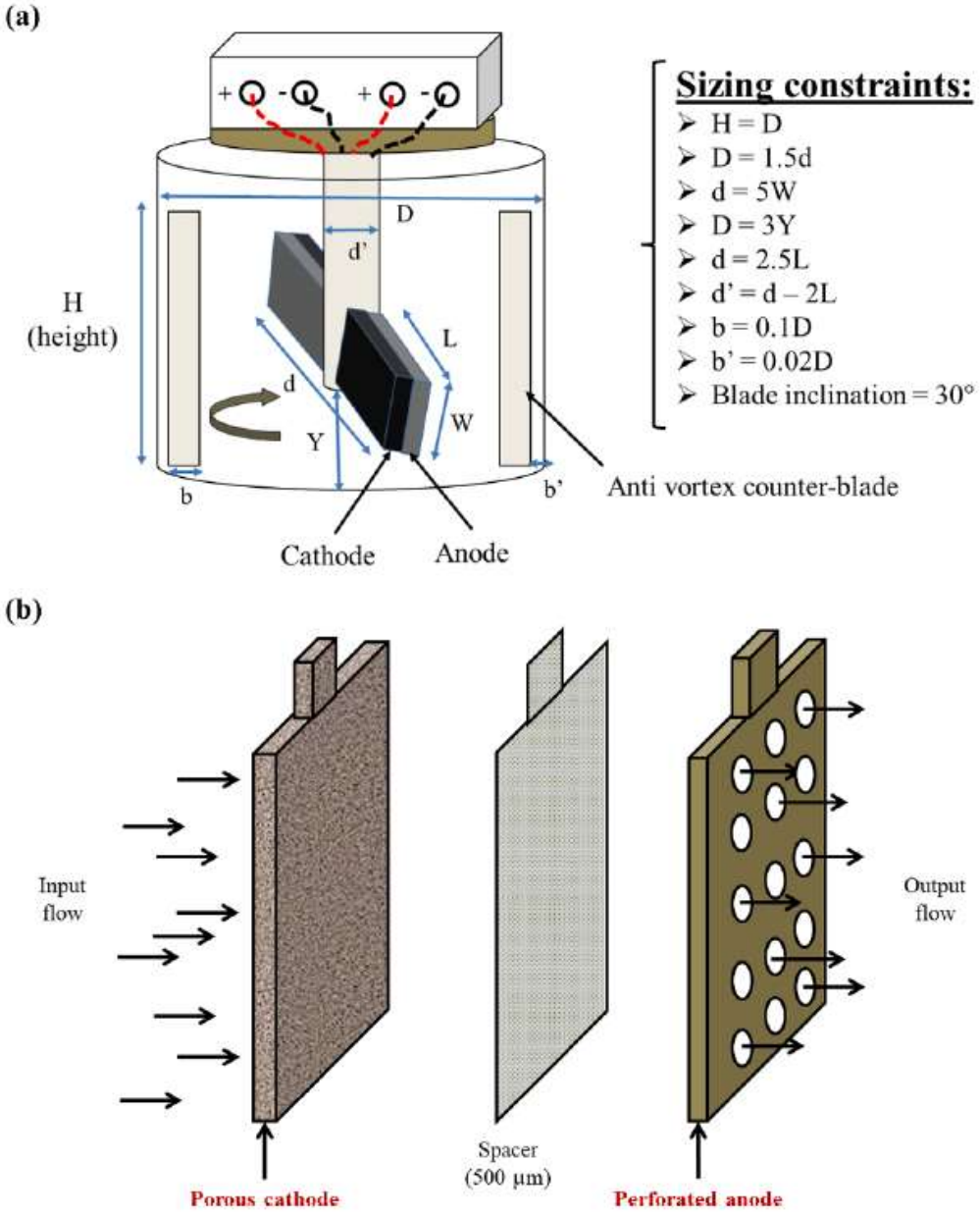

Fig. 14. **(a)** Schematic diagram of reactive electro-mixing reactor and **(b)** a reactive electro-blade acting as flow-through microreactor (Reproduced with permission from **[70]**. Copyright 2020, Elsevier).

4. Economical perspectives

Specific power consumption (E_{SP}) is typically proportional to the applied current. Depending on how much electrical current is applied for the degradation of organics, E_{SP} can be estimated for the process. It has commonly been defined as energy consumed gram of pollutant treated (kWh g-pollutant^{-1}) as written in **Eq. (13)**.

$$E_{SP} = \frac{\Delta U I t}{(\Delta C) V} \quad (13)$$

where ΔU is the cell voltage (in V), I is applied current intensity (in A), t is time of electrolysis (in s), ΔC is the decrease of pollutant concentration (in g L^{-1}) and V is the treated volume in the reactor (in L).

From a practical viewpoint, **Fig. 15** illustrates some comparisons in specific energy consumption between micro- and macroreactor setups. In agreement to **Fig. 15(a)**, Ma et al. (**Table 1**) not only observed 24% better total organic abatement but they also evaluated up to 92% drop in E_{SP} when a microreactor was adopted **[37]**. Better organic removal was attributed to mass transfer enhancement and the drop in power consumption was due to the reduction of ohmic drop in microfluidic cell **[34, 37, 53, 70]**. Moreover, further tweak in the design of microreactor could allow better energetic performance of the cell. For instance, when the whole micrometric reactor was set in motion such as proposed by Mousset **[70]** to benefit the convective transport towards electrode surface while minimizing the diffusion layer thickness on electrode, even lower E_{SP} could be obtained. According to **Fig. 15(b)**, 98% lower E_{SP} was found using microfluidic electro-mixing reactor as compared to microfluidic parallel-plate reactor with similar d_{elec}.

Therefore, with significant reduction in E_{SP}, total EAOP operational cost could heavily be cut. EAOP operating in microfluidic mode moreover with ingenious cell design could potentially be competitive with respect to other conventional methods to treat wastewater.

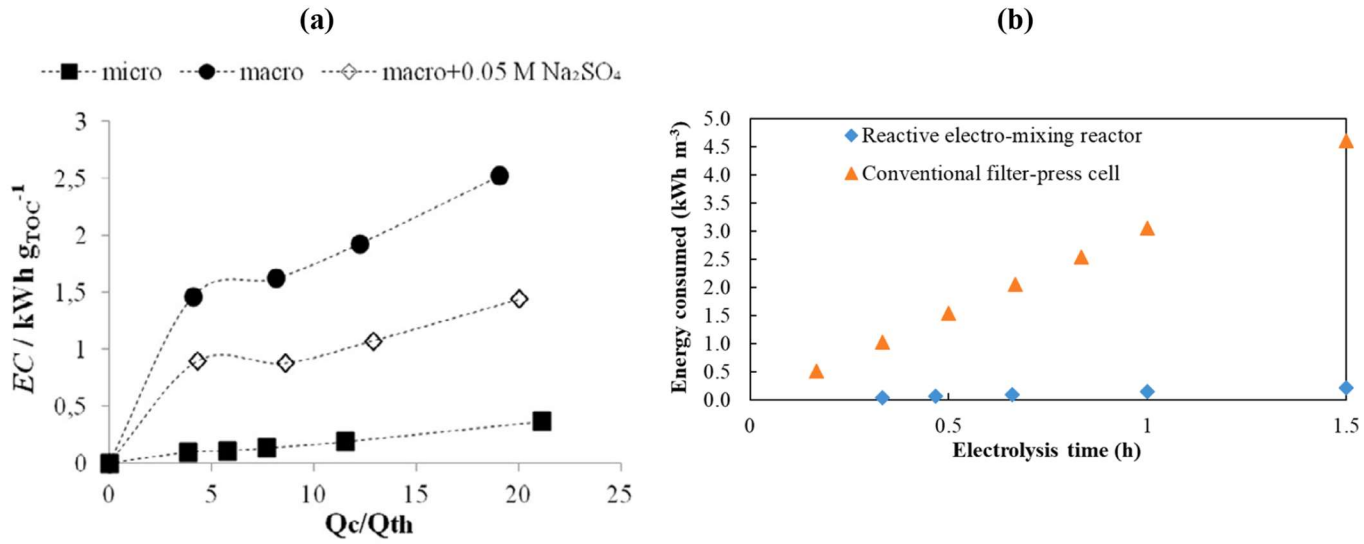

Fig. 15. Comparison of E_{SP} between **(a)** parallel-plate microreactor (d_{elec}: 50 µm) and macroreactor (d_{elec}: 2 cm, with and without supporting electrolyte) during an EO process treating real wastewater effluent using 100 mA applied current (adapted with permission from **[37]**. Copyright 2018, Elsevier) and **(b)** electro-mixing microreactor (d_{elec}: 500 µm) and microfluidic parallel-plate reactor (d_{elec}: 500 µm) during EO of synthetic effluent using 200 mA applied current (adapted with permission from **[70]**. Copyright 2020, Elsevier).

5. Summary and outlook

Considering the interest in the use of submillimetric electrochemical reactor to treat wastewater, this topic deserves more attention from research community. It offers the possibility to deal with low-conductivity effluents, while intensifying the mass transfer and therefore increasing the kinetics and process yield. Besides, power consumption can be minimized, since the cell potential is massively reduced. Given these opportunities, more evaluations on the performance of microfluidic reactors to treat real wastewater effluents are required. Moreover, increasing group of micropollutants have been identified as contaminants of concern which can cause harm to living creatures in the near future **[11]**. Consequently, prompt reliable and cost-effective complementary treatments are required sooner

rather than later. Most studies on micropollutant degradation have used an augmented concentration of the target pollutant due to analytical challenge. However, the follow up of treatment efficacy departing from actual concentrations of micropollutant detected in real effluent is essential. Next, from the practical standpoint, the improvement in treatment productivity is the utmost problematic that needs to be catered by the researchers in the domain. The opportunities offered by microfluidic cells are fruitless unless they are able to handle large effluent volumes, as recently proposed with the reactive electro-mixing reactor **[70]**. Realistically, adequate investment is needed for the installation startup. However, with proper operational maintenance on top of power saving advantage offered by submillimetric reactor feature, significant cuts in operational expense could be benefited in the long run.

To date, clogging and electrode fouling issues also represent a big hurdle for the application of microfluidic reactors at large scale **[22, 76-78]**. These challenges are more genuine when real wastewater is to be treated. Reclaimed municipal or industrial wastewater effluents often contain colloidal and suspended solids that would necessitate pretreatment steps. Recently, the occurrence of electro-precipitation in microfluidic electrochemical cell has been investigated **[36, 45]**. Care must be taken upon applying the micrometric configurations as the mass transfer was enhanced but so did the electrode fouling. Consequently, the process durability under continuous operation, which is the ultimate goal in real field applications, could massively be impacted, when regular and costly maintenance is not foreseen. Polarity reversal technique could be implemented to minimize the electro-precipitation formation such systematically applied in electrodialysis reversal at industrial scale **[79, 80]**. Nevertheless, both cathode and anode materials would need to be stable against corrosion/burning during the oxidation period and consequently the cathode material is often expensive.

Acknowledgments

Authors would like to express their sincere gratitude to the French Ministry of Higher Education and Research (MESRI) for financial grant of doctorate program for Faidzul Hakim Adnan.

References

[1] S.D. Richardson, S.Y. Kimura, Water analysis: Emerging contaminants and current issues, Analytical Chemistry, 88 (2016) 546-582.

[2] M.S. Díaz-Cruz, D. Barceló, Determination of antimicrobial residues and metabolites in the aquatic environment by liquid chromatography tandem mass spectrometry, Analytical and Bioanalytical Chemistry, 386 (2006) 973-985.

[3] M.A. Oturan, J.-J. Aaron, Advanced oxidation processes in water/wastewater treatment: Principles and applications. A review, Critical Reviews in Environmental Science and Technology, 44 (2014) 2577-2641.

[4] I. Sirés, E. Brillas, Remediation of water pollution caused by pharmaceutical residues based on electrochemical separation and degradation technologies: A review, Environment International, 40 (2012) 212-229.

[5] V. Jegatheesan, B.K. Pramanik, J. Chen, D. Navaratna, C.-Y. Chang, L. Shu, Treatment of textile wastewater with membrane bioreactor: A critical review, Bioresource Technology, 204 (2016) 202-212.

[6] M. Panizza, Chapter 13 - Fine chemical industry, pulp and paper industry, petrochemical industry and pharmaceutical industry, in: C.A. Martínez-Huitle, M.A. Rodrigo, O. Scialdone (Eds.) Electrochemical Water and Wastewater Treatment, Butterworth-Heinemann2018, pp. 335-364.

[7] K. Groenen Serrano, Chapter 6 - Indirect electrochemical oxidation using hydroxyl radical, active chlorine, and peroxodisulfate, in: C.A. Martínez-Huitle, M.A. Rodrigo, O. Scialdone (Eds.) Electrochemical Water and Wastewater Treatment, Butterworth-Heinemann2018, pp. 133-164.

[8] C. Sáez, M.A. Rodrigo, A.S. Fajardo, C.A. Martínez-Huitle, Chapter 7 - Indirect electrochemical oxidation by using ozone, hydrogen peroxide, and ferrate, in: C.A. Martínez-Huitle, M.A. Rodrigo, O. Scialdone (Eds.) Electrochemical Water and Wastewater Treatment, Butterworth-Heinemann2018, pp. 165-192.

[9] E. Brillas, I. Sirés, Chapter 11 - Hybrid and sequential chemical and electrochemical processes for water decontamination, in: C.A. Martínez-Huitle, M.A. Rodrigo, O. Scialdone (Eds.) Electrochemical Water and Wastewater Treatment, Butterworth-Heinemann2018, pp. 267-304.

[10] E. Mousset, W.H. Loh, W.S. Lim, L. Jarry, Z. Wang, O. Lefebvre, Cost comparison of advanced oxidation processes for wastewater treatment using accumulated oxygen-equivalent criteria, Water Research, 200 (2021) 117234.

[11] L. Rizzo, W. Gernjak, P. Krzeminski, S. Malato, C.S. McArdell, J.A.S. Perez, H. Schaar, D. Fatta-Kassinos, Best available technologies and treatment trains to address current challenges in urban wastewater reuse for irrigation of crops in EU countries, Science of The Total Environment, 710 (2020) 136312.

[12] P. Rychen, C. Provent, L. Pupunat, N. Hermant, Domestic and industrial water disinfection using boron-doped diamond electrodes, in: C. Comninellis, G. Chen (Eds.) Electrochemistry for the Environment, Springer New York, New York, NY, 2010, pp. 143-161.

[13] A. Kapałka, G. Fóti, C. Comninellis, Basic principles of the electrochemical mineralization of organic pollutants for wastewater treatment, in: C. Comninellis, G. Chen (Eds.) Electrochemistry for the Environment, Springer New York, New York, NY, 2010, pp. 1-23.

[14] O. Garcia-Rodriguez, E. Mousset, H. Olvera-Vargas, O. Lefebvre, Electrochemical treatment of highly concentrated wastewater: A review of experimental and modeling approaches from lab- to full-scale, Critical Reviews in Environmental Science and Technology, (2020) 1-70.

[15] O. Ganzenko, D. Huguenot, E.D. van Hullebusch, G. Esposito, M.A. Oturan, Electrochemical advanced oxidation and biological processes for wastewater treatment: A review of the combined approaches, Environmental Science and Pollution Research, 21 (2014) 8493-8524.

[16] F.C. Moreira, R.A.R. Boaventura, E. Brillas, V.J.P. Vilar, Electrochemical advanced oxidation processes: A review on their application to synthetic and real wastewaters, Applied Catalysis B: Environmental, 202 (2017) 217-261.

[17] E. Mousset, C. Trellu, H. Olvera-Vargas, Y. Pechaud, F. Fourcade, M.A. Oturan, Electrochemical technologies coupled with biological treatments, Current Opinion in Electrochemistry, 26 (2021) 100668.

[18] E. Mousset, Z. Wang, H. Olvera-Vargas, O. Lefebvre, Advanced electrocatalytic pre-treatment to improve the biodegradability of real wastewater from the electronics industry — A detailed investigation study, Journal of Hazardous Materials, 360 (2018) 552-559.

[19] E. Mousset, L. Frunzo, G. Esposito, E.D.v. Hullebusch, N. Oturan, M.A. Oturan, A complete phenol oxidation pathway obtained during electro-Fenton treatment and validated by a kinetic model study, Applied Catalysis B: Environmental, 180 (2016) 189-198.

[20] M.A. Oturan, Outstanding performances of the BDD film anode in electro-Fenton process: Applications and comparative performance, Current Opinion in Solid State and Materials Science, 25 (2021) 100925.

[21] E. Mousset, N. Oturan, M.A. Oturan, An unprecedented route of OH radical reactivity evidenced by an electrocatalytical process: Ipso-substitution with perhalogenocarbon compounds, Applied Catalysis B: Environmental, 226 (2018) 135-146.

[22] C.A. Martínez-Huitle, M.A. Rodrigo, I. Sirés, O. Scialdone, Single and coupled electrochemical processes and reactors for the abatement of organic water pollutants: A critical review, Chemical Reviews, 115 (2015) 13362-13407.

[23] I. Sirés, E. Brillas, M.A. Oturan, M.A. Rodrigo, M. Panizza, Electrochemical advanced oxidation processes: Today and tomorrow. A review, Environmental Science and Pollution Research, 21 (2014) 8336-8367.

[24] E. Mousset, L. Quackenbush, C. Schondek, A. Gerardin-Vergne, S. Pontvianne, S. Kmiotek, M.-N. Pons, Effect of homogeneous Fenton combined with electron transfer on the fate of inorganic chlorinated species in synthetic and reclaimed municipal wastewater, Electrochimica Acta, 334 (2020) 135608.

[25] E. Mousset, S. Pontvianne, M.-N. Pons, Fate of inorganic nitrogen species under homogeneous Fenton combined with electro-oxidation/reduction treatments in synthetic solutions and reclaimed municipal wastewater, Chemosphere, 201 (2018) 6-12.

[26] E. Mousset, D.D. Dionysiou, Photoelectrochemical reactors for treatment of water and wastewater: A review, Environmental Chemistry Letters, 18 (2020) 1301-1318.

560 [27] A. Wang, Y.-Y. Li, A.L. Estrada, Mineralization of antibiotic sulfamethoxazole by photoelectro-Fenton
561 treatment using activated carbon fiber cathode and under UVA irradiation, Applied Catalysis B:
562 Environmental, 102 (2011) 378-386.

563 [28] M. Skoumal, R.M. Rodríguez, P.L. Cabot, F. Centellas, J.A. Garrido, C. Arias, E. Brillas, Electro-Fenton,
564 UVA photoelectro-Fenton and solar photoelectro-Fenton degradation of the drug ibuprofen in acid aqueous
565 medium using platinum and boron-doped diamond anodes, Electrochimica Acta, 54 (2009) 2077-2085.

566 [29] O. Scialdone, A. Galia, S. Sabatino, Abatement of Acid Orange 7 in macro and micro reactors. Effect of
567 the electrocatalytic route, Applied Catalysis B: Environmental, 148-149 (2014) 473-483.

568 [30] S. Sabatino, A. Galia, O. Scialdone, Electrochemical abatement of organic pollutants in continuous-
569 reaction systems through the assembly of microfluidic cells in series, ChemElectroChem, 3 (2016) 83-90.

570 [31] E. Mousset, Interest of micro-reactors for the implementation of advanced electrocatalytic oxidation with
571 boron-doped diamond anode for wastewater treatment, Current Opinion in Electrochemistry, (2021) 100897.

572 [32] J.F. Pérez, J. Llanos, C. Sáez, C. López, P. Cañizares, M.A. Rodrigo, A microfluidic flow-through
573 electrochemical reactor for wastewater treatment: A proof-of-concept, Electrochemistry Communications, 82
574 (2017) 85-88.

575 [33] O. Scialdone, C. Guarisco, A. Galia, Oxidation of organics in water in microfluidic electrochemical
576 reactors: Theoretical model and experiments, Electrochimica Acta, 58 (2011) 463-473.

577 [34] J.F. Pérez, J. Llanos, C. Sáez, C. López, P. Cañizares, M.A. Rodrigo, Development of an innovative
578 approach for low-impact wastewater treatment: A microfluidic flow-through electrochemical reactor,
579 Chemical Engineering Journal, 351 (2018) 766-772.

580 [35] F.H. Adnan, M.-N. Pons, E. Mousset, Mass transport evolution in microfluidic thin film electrochemical
581 reactors: New correlations from millimetric to submillimetric interelectrode distances, Electrochemistry
582 Communications, 130 (2021) 107097.

583 [36] F.H. Adnan, S. Pontvianne, M.-N. Pons, E. Mousset, Unprecedented roles of submillimetric interelectrode
584 distances and electrogenerated gas bubbles on mineral cathodic electro-precipitation: Modeling and interface
585 studies, Chemical Engineering Journal, (2021) 133413.

586 [37] P. Ma, H. Ma, S. Sabatino, A. Galia, O. Scialdone, Electrochemical treatment of real wastewater. Part 1:
587 Effluents with low conductivity, Chemical Engineering Journal, 336 (2018) 133-140.

588 [38] O. Scialdone, E. Corrado, A. Galia, I. Sirés, Electrochemical processes in macro and microfluidic cells
589 for the abatement of chloroacetic acid from water, Electrochimica Acta, 132 (2014) 15-24.

590 [39] W. Khongthon, G. Jovanovic, A. Yokochi, P. Sangvanich, V. Pavarajarn, Degradation of diuron via an
591 electrochemical advanced oxidation process in a microscale-based reactor, Chemical Engineering Journal, 292
592 (2016) 298-307.

593 [40] S. Fransen, J. Fransaer, S. Kuhn, Current and concentration distributions in electrochemical microreactors:
594 Numerical calculations and asymptotic approximations for self-supported paired synthesis, Electrochimica
595 Acta, 292 (2018) 914-934.

596 [41] E. Mousset, Y. Pechaud, N. Oturan, M.A. Oturan, Charge transfer/mass transport competition in advanced
597 hybrid electrocatalytic wastewater treatment: Development of a new current efficiency relation, Applied
598 Catalysis B: Environmental, 240 (2019) 102-111.

599 [42] O. Scialdone, A. Galia, S. Sabatino, Electro-generation of H2O2 and abatement of organic pollutant in
600 water by an electro-Fenton process in a microfluidic reactor, Electrochemistry Communications, 26 (2013) 45-
601 47.

[43] M. Rodríguez, M. Muñoz-Morales, J.F. Perez, C. Saez, P. Cañizares, C.E. Barrera-Díaz, M.A. Rodrigo, Toward the development of efficient electro-Fenton reactors for soil washing wastes through microfluidic cells, Industrial & Engineering Chemistry Research, 57 (2018) 10709-10717.

[44] O. Scialdone, A. Galia, C. Guarisco, S. La Mantia, Abatement of 1,1,2,2-tetrachloroethane in water by reduction at silver cathode and oxidation at boron doped diamond anode in micro reactors, Chemical Engineering Journal, 189-190 (2012) 229-236.

[45] F.H. Adnan, E. Mousset, S. Pontvianne, M.-N. Pons, Mineral cathodic electro-precipitation and its kinetic modelling in thin-film microfluidic reactor during advanced electro-oxidation process, Electrochimica Acta, 387 (2021) 138487.

[46] M. Panizza, G. Cerisola, Direct and mediated anodic oxidation of organic pollutants, Chemical Reviews, 109 (2009) 6541-6569.

[47] M. Panizza, C.A. Martinez-Huitle, Role of electrode materials for the anodic oxidation of a real landfill leachate – Comparison between Ti–Ru–Sn ternary oxide, PbO2 and boron-doped diamond anode, Chemosphere, 90 (2013) 1455-1460.

[48] O. Scialdone, C. Guarisco, A. Galia, G. Filardo, G. Silvestri, C. Amatore, C. Sella, L. Thouin, Anodic abatement of organic pollutants in water in micro reactors, Journal of Electroanalytical Chemistry, 638 (2010) 293-296.

[49] O. Scialdone, A. Galia, S. Sabatino, D. Mira, C. Amatore, Electrochemical conversion of dichloroacetic acid to chloroacetic acid in a microfluidic stack and in a series of microfluidic reactors, ChemElectroChem, 2 (2015) 684-690.

[50] S.B. Kacem, D. Clematis, S.C. Elaoud, A. Barbucci, M. Panizza, A flexible electrochemical cell setup for pollutant oxidation in a wide electrical conductivity range and its integration with ultrasound, Journal of Water Process Engineering, 46 (2022) 102564.

[51] J.F. Pérez, J. Llanos, C. Sáez, C. López, P. Cañizares, M.A. Rodrigo, On the design of a jet-aerated microfluidic flow-through reactor for wastewater treatment by electro-Fenton, Separation and Purification Technology, 208 (2019) 123-129.

[52] J.F. Pérez, J. Llanos, C. Sáez, C. López, P. Cañizares, M.A. Rodrigo, Towards the scale up of a pressurized-jet microfluidic flow-through reactor for cost-effective electro-generation of H2O2, Journal of Cleaner Production, 211 (2019) 1259-1267.

[53] E. Mousset, M. Puce, M.N. Pons, Advanced electro-oxidation with boron-doped diamond for acetaminophen removal from real wastewater in a microfluidic reactor: Kinetics and mass-transfer studies, ChemElectroChem, 6 (2019) 2908-2916.

[54] A.Y. Bagastyo, D.J. Batstone, I. Kristiana, W. Gernjak, C. Joll, J. Radjenovic, Electrochemical oxidation of reverse osmosis concentrate on boron-doped diamond anodes at circumneutral and acidic pH, Water Research, 46 (2012) 6104-6112.

[55] S. Garcia-Segura, E. Mostafa, H. Baltruschat, Could NOx be released during mineralization of pollutants containing nitrogen by hydroxyl radical? Ascertaining the release of N-volatile species, Applied Catalysis B: Environmental, 207 (2017) 376-384.

[56] Y. Ouarda, C. Trellu, G. Lesage, M. Rivallin, P. Drogui, M. Cretin, Electro-oxidation of secondary effluents from various wastewater plants for the removal of acetaminophen and dissolved organic matter, Science of The Total Environment, 738 (2020) 140352.

[57] C.A. Cid, J.T. Jasper, M.R. Hoffmann, Phosphate recovery from human waste via the formation of hydroxyapatite during electrochemical wastewater treatment, ACS Sustainable Chemistry & Engineering, 6 (2018) 3135-3142.

[58] T.R. Devlin, M.S. Kowalski, E. Pagaduan, X. Zhang, V. Wei, J.A. Oleszkiewicz, Electrocoagulation of wastewater using aluminum, iron, and magnesium electrodes, Journal of Hazardous Materials, 368 (2019) 862-868.

[59] S. Garcia-Segura, J. Keller, E. Brillas, J. Radjenovic, Removal of organic contaminants from secondary effluent by anodic oxidation with a boron-doped diamond anode as tertiary treatment, Journal of Hazardous Materials, 283 (2015) 551-557.

[60] S. Garcia-Segura, E. Mostafa, H. Baltruschat, Electrogeneration of inorganic chloramines on boron-doped diamond anodes during electrochemical oxidation of ammonium chloride, urea and synthetic urine matrix, Water Research, 160 (2019) 107-117.

[61] P. Vanysek, Electrochemical series, CRC Handbook of Chemistry and Physics2005, pp. 23.

[62] M.E.H. Bergmann, J. Rollin, Product and by-product formation in laboratory studies on disinfection electrolysis of water using boron-doped diamond anodes, Catalysis Today, 124 (2007) 198-203.

[63] M.E.H. Bergmann, J. Rollin, T. Iourtchouk, The occurrence of perchlorate during drinking water electrolysis using BDD anodes, Electrochimica Acta, 54 (2009) 2102-2107.

[64] C. Deslouis, I. Frateur, G. Maurin, B. Tribollet, Interfacial pH measurement during the reduction of dissolved oxygen in a submerged impinging jet cell, Journal of Applied Electrochemistry, 27 (1997) 482-492.

[65] H. Deligianni, L.T. Romankiw, In situ surface pH measurement during electrolysis using a rotating pH electrode, IBM Journal of Research and Development, 37 (1993) 85-95.

[66] Y. Lei, B. Song, R.D. van der Weijden, M. Saakes, C.J.N. Buisman, Electrochemical induced calcium phosphate precipitation: Importance of local pH, Environmental Science & Technology, 51 (2017) 11156-11164.

[67] C. Deslouis, D. Festy, O. Gil, V. Maillot, S. Touzain, B. Tribollet, Characterization of calcareous deposits in artificial sea water by impedances techniques: 2-deposit of Mg(OH)2 without CaCO3, Electrochimica Acta, 45 (2000) 1837-1845.

[68] L. Beaunier, C. Gabrielli, G. Poindessous, G. Maurin, R. Rosset, Investigation of electrochemical calcareous scaling: Nuclei counting and morphology, Journal of Electroanalytical Chemistry, 501 (2001) 41-53.

[69] C. Deslouis, D. Festy, O. Gil, G. Rius, S. Touzain, B. Tribollet, Characterization of calcareous deposits in artificial sea water by impedance techniques — 1. Deposit of CaCO3 without Mg(OH)2, Electrochimica Acta, 43 (1998) 1891-1901.

[70] E. Mousset, Unprecedented reactive electro-mixing reactor: Towards synergy between micro- and macro-reactors?, Electrochemistry Communications, 118 (2020) 106787.

[71] J.A. Alden, R.G. Compton, Hydrodynamic voltammetry with channel microband electrodes: axial diffusion effects, Journal of Electroanalytical Chemistry, 404 (1996) 27-35.

[72] R.G. Compton, P.R. Unwin, Channel and tubular electrodes, Journal of Electroanalytical Chemistry and Interfacial Electrochemistry, 205 (1986) 1-20.

[73] J.A. Cooper, R.G. Compton, Channel electrodes — A review, Electroanalysis, 10 (1998) 141-155.

[74] C.A. Martinez-Huitle, S. Ferro, A. De Battisti, Electrochemical incineration of oxalic acid: Reactivity and engineering parameters, Journal of Applied Electrochemistry, 35 (2005) 1087-1093.

685 [75] M. Cruz-Díaz, F.F. Rivera, E.P. Rivero, I. González, The FM01-LC reactor modeling using axial
686 dispersion model with a reaction term coupled with a continuous stirred tank (CST), Electrochimica Acta, 63
687 (2012) 47-54.

688 [76] I. Sanjuán, D. Benavente, V. García-García, E. Expósito, V. Montiel, Electrochemical softening of
689 concentrates from an electrodialysis brackish water desalination plant: Efficiency enhancement using a three-
690 dimensional cathode, Separation and Purification Technology, 208 (2019) 217-226.

691 [77] Y. Yu, H. Jin, X. Quan, B. Hong, X. Chen, Continuous multistage electrochemical precipitation reactor
692 for water softening, Industrial & Engineering Chemistry Research, 58 (2019) 461-468.

693 [78] Y. Yu, H. Jin, X. Jin, R. Yan, L. Zhang, X. Chen, Current pulsated electrochemical precipitation for water
694 softening, Industrial & Engineering Chemistry Research, 57 (2018) 6585-6593.

695 [79] F. Valero, R. Arbós, Desalination of brackish river water using Electrodialysis Reversal (EDR): Control
696 of the THMs formation in the Barcelona (NE Spain) area, Desalination, 253 (2010) 170-174.

697 [80] K.-H. Yeon, J.-H. Song, J. Shim, S.-H. Moon, Y.-U. Jeong, H.-Y. Joo, Integrating electrochemical
698 processes with electrodialysis reversal and electro-oxidation to minimize COD and T-N at wastewater
699 treatment facilities of power plants, Desalination, 202 (2007) 400-410.

700

701

Conflict of Interest Statement

Manuscript title: Thin film microfluidic reactors in electrochemical advanced oxidation processes for wastewater treatment: A review on influencing parameters, scaling issues and engineering considerations

The authors whose names are listed immediately below certify that they have NO affiliations with or involvement in any organization or entity with any financial interest (such as honoraria; educational grants; participation in speakers' bureaus; membership, employment, consultancies, stock ownership, or other equity interest; and expert testimony or patent-licensing arrangements), or non-financial interest (such as personal or professional relationships, affiliations, knowledge or beliefs) in the subject matter or materials discussed in this manuscript.

Authors names:

Faidzul Hakim Adnan, Marie-Noëlle Pons, Emmanuel Mousset